Tonkie Khimicheskie Tekhnologii = Fine Chemical Technologies.
2025;20(4):324–343 ISSN 2686-7575 (Online)

UDC 546.62+535.376
https://doi.org/10.32362/2410-6593-2025-20-4-324-343
EDN KEDCJH

REVIEW ARTICLE

Aluminum oxynitrides doped with rare-earth and transition metal ions

Nailya S. Akhmadullina[1], ✉, Aleksey V. Ishchenko[2]

[1] *A.A. Baikov Institute of Metallurgy and Material Science, Russian Academy of Sciences, Moscow, 119991 Russia*

[2] *Ural Federal University, Yekaterinburg, 620062 Russia*

✉ *Corresponding author, e-mail: nakhmadullina@mail.ru*

Abstract

Objectives. The work set out to summarize the results of the studies of aluminum oxynitrides (AlONs) doped with rare earth (REM) and transition metals (TM) and to highlight the main effects of REM and TM dopants on the formation, phase composition, and optical properties of the AlON.

Results. The presented analysis of the literature data includes the results of our own studies of the AlON doped with REM and TM ions. The influence of REM and TM additives on the formation of AlON and its phase com position, as well as optical properties, was considered.

Conclusions. It is clearly shown that the doping with REM and TM ions enhances the formation of pure AlON phase via high-temperature synthesis from oxide and nitride. The oxynitride matrix exhibits reducing properties with respect to both REM and TM. Doping with the REM ions leads to the emergence of luminescent properties in the visible range, while doping with TM ions affects the band gap in AlON as a semiconductor. The solubility limits of all metals in the AlON matrix do not exceed 1–2 at. % vs Al. Concentration quenching of luminescence is observed at REM contents from 0.1 to 0.5 at. %.

Keywords

aluminum oxynitride, rare earth metals, transition metals, phase composition, solubility, luminescence

Submitted: 02.10.2024
Revised: 27.01.2025
Accepted: 15.06.2025

For citation

Akhmadullina N.S., Ishchenko A.V. Aluminum oxynitrides doped with rare-earth and transition metal ions. *Tonk. Khim. Tekhnol. = Fine Chem. Technol*. 2025;20(4):324–343. https://doi.org/10.32362/2410-6593-2025-20-4-324-343

ОБЗОР

Оксинитриды алюминия, легированные ионами редкоземельных и переходных металлов

Н.С. Ахмадуллина[1],✉, А.В. Ищенко[2]

[1] *Институт металлургии и материаловедения им. А.А. Байкова, Российская академия наук, Москва, 119991 Россия*

[2] *Уральский федеральный университет им. первого Президента России Б.Н. Ельцина, Екатеринбург, 620062 Россия*

✉ *Автор для переписки, e-mail: nakhmadullina@mail.ru*

Аннотация

Цели. Обобщить результаты исследований и сформулировать основные закономерности влияния ионов редкоземельных (РЗМ) и переходных металлов (ПМ) на формирование, фазовый состав и оптические свойства оксинитрида алюминия (алона).

Результаты. Проведен анализ литературных данных, включая результаты собственных исследований авторов, касающихся алонов, легированных ионами РЗМ и ПМ. Рассмотрено влияние добавок РЗМ и ПМ на формирование алона и его фазовый состав и оптические свойства.

Выводы. Установлено, что введение ионов РЗМ и ПМ способствует образованию фазы алона при высокотемпературном синтезе из оксида и нитрида алюминия. Оксинитридная матрица проявляет восстановительные свойства как в отношении РЗМ, так и ПМ. Легирование ионами РЗМ приводит к получению материалов, обладающих люминесцентными свойствами в видимом диапазоне. Легирование ионами ПМ влияет на ширину запрещенной зоны алона как полупроводника. Пределы растворимости всех металлов в матрице алона не превышают 1–2 ат. % относительно алюминия. Концентрационное тушение люминесценции наблюдается при содержании РЗМ от 0.1 до 0.5 ат. %.

Ключевые слова

оксинитрид алюминия, редкоземельные металлы, переходные металлы, фазовый состав, растворимость, люминесценция

Поступила: 02.10.2024
Доработана: 27.01.2025
Принята в печать: 15.06.2025

Для цитирования

Ахмадуллина Н.С., Ищенко А.В. Оксинитриды алюминия, легированные ионами редкоземельных и переходных металлов. *Тонкие химические технологии*. 2025;20(4):324–343. https://doi.org/10.32362/2410-6593-2025-20-4-324-343

INTRODUCTION

Aluminum oxide in its trigonal modification α-Al_2O_3, also known as corundum, has found wide application due to its thermal and chemical resistance, as well as desired physical and mechanical characteristics of hardness and strength [1]. The next generation material in relation to aluminum oxide is aluminum oxynitride, otherwise called AlON. AlON has been known since about 1960–1970, when the phase diagram of the pseudo-binary AlN–Al_2O_3 system was fully described [2–5]. The classical phase diagram of this system, which is constructed under the assumption that the atmosphere is a nitrogen current, was first presented in [6]. According to these data, AlON is a solid solution in the AlN–Al_2O_3 system with a rather wide region of homogeneity. The γ-AlON phase has a spinel-type crystal structure (space group $Fd\bar{3}m$). As a phase of variable composition $Al_{64+x/3}O_{32-x}N_x$ ($0 < x < 8$), it is usually considered in the model of constant anions, as proposed by McCauley [3]. Its stoichiometric composition in this case (at $x = 5$) is defined by the formula $Al_{23}O_{27}N_5$ ($5AlN{\cdot}9Al_2O_3$). In this model, it is assumed that the anionic positions are completely occupied by oxygen and nitrogen in the crystal lattice of the spinel phase, while the cationic positions are occupied by aluminum and contain vacancies. Comparatively recent quantum-chemical modeling has confirmed the assumption of this type of structure as the most probable [7]. The indicated composition corresponds to the content of AlN 35.7 mol % and Al_2O_3 64.3 mol %. Another frequently attributed composition, which is described by the formula Al_5O_6N ($AlN{\cdot}2Al_2O_3$), corresponds to the content of AlN 33.3 mol % and Al_2O_3 66.7 mol %. The exact composition depends on the initial components and the method of synthesis. In addition to γ-AlON in the system, there are a number of mixed oxide-nitride phases in which aluminum nitride predominates and which are thus considered as AlN polytypes: 27R ($7AlN{\cdot}Al_2O_3$), 21R ($5AlN{\cdot}Al_2O_3$), 12H ($4AlN{\cdot}Al_2O_3$) and others

(symbols R and H denote rhombohedral and hexagonal phases, respectively). On the other hand, there are oxonitride phases of composition $Al_{11}O_{15}N$ (ϕ′-AlON, $AlN{\cdot}5Al_2O_3$) and $Al_{27}O_{39}N$ (ϕ-AlON, $AlN{\cdot}13Al_2O_3$).

Among all these phases, it is γ-AlON that inherits the high thermal and chemical stability and strength of corundum, adding to them resistance to high-speed loading, due to which it has attracted the attention of researchers over the last five decades [8, 9]. Among the many applications of alumina are the production of transparent ceramics [5] and its use as a phosphor matrix for the fabrication of light-emitting diodes (LEDs), including white light-emitting diodes (WLEDs) [10], which currently demonstrate longer lifetimes, higher light output and lower power consumption as compared to other light sources, as well as being more environmentally friendly [11–13]. Currently, commercially available WLEDs can be fabricated by combining an InGaN chip with emission in the blue range of the spectrum and a yellow phosphor $Y_3Al_5O_{12}$ (YAG:Ce) phosphor [14]. However, this type of WLED has a low color rendering index and high correlated color temperature (CCT) due to the lack of sufficient emission in the red region [15, 16]. To solve this problem, WLEDs based on tri-color phosphors and LEDs emitting in the near ultraviolet (UV) region have been developed. This approach is considered to be the most promising because due to the excellent color rendering and low CCT demonstrateed by WLEDs at high efficiency [17, 18]. The search for new luminescent materials that provide luminescence in the red, blue and green spectral regions is relevant.

AlON in powder form is usually obtained by reaction between AlN and Al_2O_3 powders with some additives. This reaction can be accomplished by plasma arc synthesis, carbothermal reduction, or self-propagating high-temperature synthesis [5, 19–21]. For fabrication, the resulting AlON powder is molded and sintered at temperatures >1850°C for a long time in a nitrogen atmosphere (by pressureless sintering) and by hot pressing, hot isostatic pressing, or reaction sintering [22]. The use of transient liquid-phase sintering, in which the material moves from the liquid/solid state region to the solid solution region as the liquid reacts with and is incorporated into the AlON phase as it compacts, has also been investigated [5, 23].

Aluminum oxynitrides doped with REM ions

Aluminum oxynitride can be doped with various metal ions to impart certain properties. Doping with REM ions is used to improve physical and mechanical properties, as well as to impart luminescent properties to AlON. In particular, the incorporation of Y^{3+} and La^{3+} ions into AlON contributes to the densification of the material at the sintering stage [24–30]. Martin *et al*. used 0.5 wt % Y_2O_3 as a sintering additive to densify and enhance the homogeneity at the microstructure level of AlON by hot pressing [25]. Similarly, Wang *et al*. prepared transparent AlON ceramics (2 mm thick) using 0.12 wt % Y_2O_3 and 0.09 wt % La_2O_3 as sintering additives, achieving a transmittance of ~84% at 1100 nm for a 4.2 mm thick sample after hot isostatic pressing for 2 h at 1900°C [26]. Nevertheless, this ceramic is characterized by large grains because at this temperature, grain growth is not only due to compaction but also stimulated by additives [27]. The developed method was further improved [29], and transparent AlON ceramics with similar characteristics were obtained with lower content of sintering additives—0.08 wt % Y_2O_3 and 0.02 wt % La_2O_3. Addition of extra 0.2 wt % MgO allowed obtaining compact material from AlON powder by pressureless sintering at 1900°C for 24 h, and the relative density of the obtained sample amounted to 99.9% [30]. Jin *et al*. also sintered AlON without pressure using 0.08 wt % Y_2O_3, 0.025 wt % La_2O_3, and 0.1 wt % MgO as additives. The resulting 1 mm thick sample had a transmittance of ~81% at a wavelength of 1100 nm [25].

The inclusion of other REMs into the composition of AlON, as well as certain TMs, primarily Mn^{2+}, is used to impart luminescent properties to the sample [31, 32]. Doping with Eu^{2+} ions allows the preparation of blue-green light phosphors. Kikkawa *et al*. [33] reported the synthesis of AlON:Eu^{2+} phosphors via ammonia nitriding of aluminum oxide prepared from aluminum nitrate by sol–gel method with the addition of europium nitrate. The synthesis included nitriding steps, which were carried out at 1200–1500°C, and post-annealing in a nitrogen current at 1700°C. Powders with Eu^{2+} content of 1 and 3 mol % showed two maxima in the photoluminescence (PL) spectrum at 475 and 520 nm, whose source was presumably the $EuAl_2O_4$ phase. Subsequently, co-alloyed phosphors of the composition AlON:3% Eu^{2+}/10% Mg^{2+} were obtained by solid-phase synthesis directly from commercial Al_2O_3 and AlN powders by firing in a nitrogen current at 1800°C [34]. The obtained phosphors exhibited a broad emission band in the PL spectra in the range of 430–620 nm with a maximum around 490 nm at the excitation wavelength of 310 nm. It was clarified that the main europium-containing phase in the samples of AlON doped with Eu^{2+} ions is the europium aluminate phase of the composition $EuAl_{12}O_{19}$. Samples with similar composition and properties with Eu^{2+} content of 0.6% and 0.8% were prepared by carbothermal reductive nitriding of aluminum oxide [35]. The obtained samples were effectively excited by UV light with a wavelength of

350–410 nm and had an emission band in the PL spectrum with a maximum around 495 nm. The authors also determined the dynamic characteristics of luminescence and studied the dependence of luminescence intensity in the temperature range from 80 to 500 K. The effect of thermal quenching of luminescence was observed in the range of 200–500 K. Similar results were obtained in [36]. AlON:*x*%Eu (x = 0.25–1.00) phosphors showed two main emission bands in the PL spectrum with maxima at 410 and 475 nm. The intensity of the 475 nm band reached a plateau at x = 0.25% and above, probably due to reaching the solubility limit of the Eu^{2+} ion in the AlON matrix. The intensity of the 410 nm band increased linearly with increasing Eu^{2+} content, which was mainly due to the contribution of the $EuAl_{12}O_{19}$ phase.

In previous works, we carried out detailed studies of pulsed cathodoluminescence (PCL) as well as PL for a wide range of luminophores based on AlN doped with REM ions. A synthesis method based on the interaction of amorphous highly dispersed Al_2O_3 with AlN in a pressureless nitrogen current at a temperature of 1600–1750°C was developed. Amorphous highly dispersed Al_2O_3 was prepared by controlled hydrolysis of aluminum isopropoxide $Al(OiPr)_3$ in an isopropanol–water mixture in the presence of citric acid with the addition of magnesium acetate (Mg^{2+} content is <1 at. % relative to aluminum) followed by drying and annealing in air. The use of Al_2O_3 obtained in this way avoids the need for increased nitrogen pressure (a small current of N_2 at a pressure of 1 atm is sufficient) to achieve a decrease in the synthesis temperature by a value from 100 to 350°C, as well as to reduce the time of high-temperature processing to 1–2 h. Furthermore, the doping ion (or ions) can be introduced in the form of water- or organosoluble compounds at the stage of aluminum isopropoxide synthesis, allowing, in some cases, to solve the problem of poor homogenization of the mixture at low contents of doping ions. Using the developed method, AlON doped with Eu^{2+}, Ce^{3+} [37] and Tb^{3+} ions [38], as well as those doped with Eu^{2+}/Ce^{3+}, Eu^{2+}/Tb^{3+}, and Ce^{3+}/Tb^{3+} ion pairs, were synthesized [39].

Eu^{2+} and Ce^{3+} doped AlON were prepared by two methods: using as a source of REM ions the corresponding oxides added to a mixture of amorphous highly dispersed Al_2O_3 and AlN, and the use of REM acetylacetonates for doping Al_2O_3, which was further subjected to high-temperature sintering in a nitrogen current in a mixture with AlN [37]. The Eu^{2+} content varied in the range of 0.025–1.0 at. % and Ce^{3+} content varied in the range of 0.025–0.2 at. %. The annealing was carried out at 1600°C for 2 h. All obtained AlON:REM samples are mixtures of aluminum oxynitride Al_5O_6N, corundum α-Al_2O_3 and impurities AlN and REM aluminates. The content of these phases depends on the concentration and nature of the alloying ions and the synthesis procedure. When AlON:REM is obtained directly from Al_2O_3, AlN, and Eu_2O_3 or CeO_2 at all concentrations of REM ions, the content of impurity phases does not exceed 5–7 vol %. On the contrary, in the case of pre-doping of Al_2O_3 with REM acetylacetonates at low concentrations of Eu^{2+} and Ce^{3+}, the phases of Al_2O_3 and AlN are minor, but they cannot be considered as impurity phases, since their content reaches tens of vol %. When the concentrations of Eu^{2+} and Ce^{3+} increase to a certain level (0.2 and 0.1 at. %, respectively), the content of minor phases sharply decreases. For the series obtained using Eu_2O_3 and CeO_2, the lowest impurity content is observed at close Eu^{2+} and Ce^{3+} contents, respectively, and the impurity content is markedly lower compared to the series obtained using $Eu(acac)_3$ and $Ce(acac)_3$. With further increase in Eu^{2+} and Ce^{3+} concentrations, the formation of REM aluminates $EuAl_{12}O_{19}$ and $CeAl_{11}O_{18}$ is observed. The formation of $(REM)Al_xO_y$ is usually accompanied by an increase in AlN content. It can be assumed that the figurative point shifts to the region of ternary systems AlON + $CeAl_{11}O_{18}/EuAl_{12}O_{19}$ + AlN as a result of Al_2O_3 consumption for the formation of $(REM)Al_xO_y$.

The PCL spectra of the series samples obtained using Eu_2O_3 and $Eu(acac)_3$ are presented in Fig. 1. For both series, broad bands of complex shape with maximum in the range of 422–505 nm are observed depending on the Eu^{2+} concentration and precursor type. The highest intensity in both series is exhibited by samples with Eu^{2+} content of 0.5 at. %. The PCL spectra of samples with Eu^{2+} concentration of 0.4, 0.5, and 1.0 at. % have a flat top due to saturation of the photodetector during measurement (Fig. 1a).

The PCL spectra of the series samples prepared using Eu_2O_3 show pronounced *d*→*f*-luminescence bands of Eu^{2+} with a maximum in the region of 495–510 nm at Eu^{2+} concentrations from 0.4 to 1.0 at. % (Fig. 1a). When the Eu^{2+} concentration increases from 0.025 to 1.0 at. %, the maximum of the luminescence band undergoes a bathochromic shift due to the increase in the Eu^{2+} luminescence intensity against the background of the intrinsic broadband luminescence bands of AlON and impurities α-Al_2O_3 [40] and AlN [41], whose maxima lie in the range of 400–420 nm. The PCL spectra of a series of samples obtained using $Eu(acac)_3$ differ from those discussed above (Fig. 1b). The emission intensity of the samples prepared using $Eu(acac)_3$ is lower than for the samples synthesized using Eu_2O_3. With increasing Eu^{2+} concentration, the highest luminescence intensity is observed at an Eu^{2+} ion content of 0.5 at. %, as for the samples prepared using Eu_2O_3; however, the *d*→*f*-luminescence bands of Eu^{2+} appear as a broad band shoulder with a maximum around 450 nm. The latter

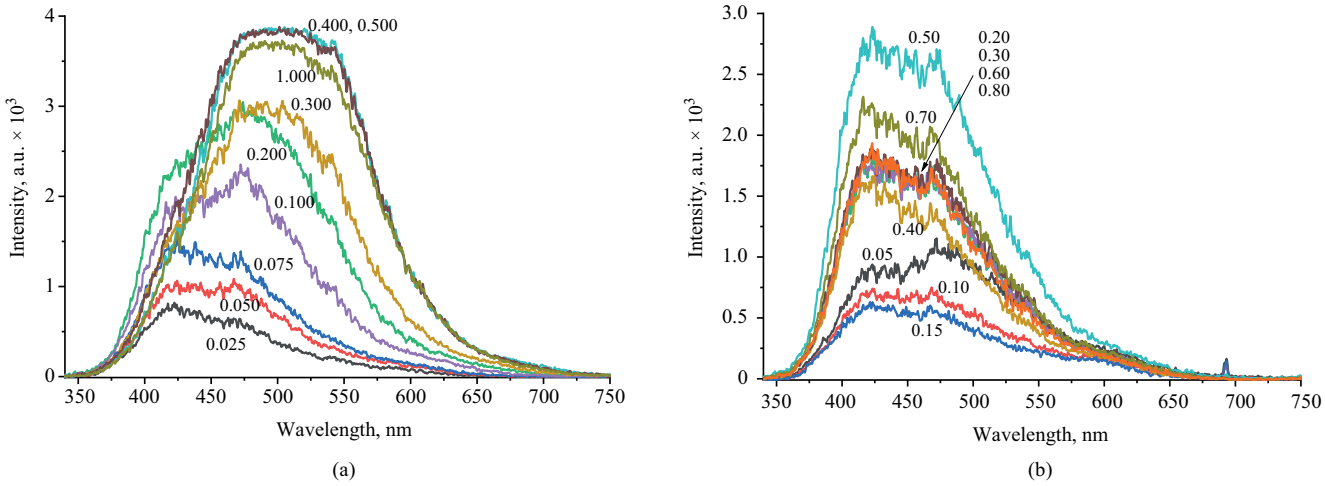

Fig. 1. Pulsed cathodoluminescence (PCL) spectra of Eu^{2+}-doped AlON prepared with Eu_2O_3 (a) and $Eu(acac)_3$ (b). The concentration in at. % of Eu ions is shown near the curves (reprinted from [37])

may be due to defects in the crystal structure of Al_5O_6N, which are vacancies in the anionic sublattice and O_N- and (V_{Al}-O_N)-type centers [42]. It is also contributed by the intrinsic emission of impurities α-Al_2O_3 [40] and AlN [41].

The PCL spectra of a series of samples obtained using Eu_2O_3 at Eu^{2+} content less than 0.1 at. % and those of all samples obtained using $Eu(acac)_3$ can be described as the sum of emission bands of AlN (400, 475, and 600 nm [41]) and F-centers in α-Al_2O_3 (410–420 nm) [40]. It can be assumed that similar defects exist in Al_5O_6N.

A comparatively recent theoretical study of the geometrical and electronic structure and its relation to the optical properties of γ-AlON doped with Eu^{2+} ions has been performed [43]. The calculations were performed using the CASTEP software package[1]. The model of permanent anions was used for the AlON structure [3]. Eu^{2+} anions can occupy one of 4 possible positions: tetrahedral positions $V_{Al}O_4$ and $V_{Al}O_3N$ and octahedral positions $V_{Al}O_6$ and $V_{Al}O_5N$. Calculations have shown that for Eu^{2+} ions the octahedral positions of $V_{Al}O_5N$ are preferable. The lattice parameters and primitive cell volume of $Eu_xAl_{23-x}O_{27}N_5$ increase with increasing Eu^{2+} content. In the calculated absorption spectrum of PL $Al_{23}O_{27}N_5$ doped with Eu^{2+}, an intense band in the range 275–425 nm with a maximum at 335 nm was observed, which was attributed to electronic transitions $4f^7 \rightarrow 4f^6 5d^1$ in the Eu^{2+} ion, and the position of which agrees quite well with the experimental data. However, it should be taken into account that calculations in the framework of the density functional theory lead to a systematic underestimation of the optical gap width. In this case, the calculations gave a value of 4.03 eV for the unalloyed AlON, while the experimentally determined value is 6.2–6.5 eV [44, 45].

The PCL spectra of a series of samples obtained using CeO_2 and $Ce(acac)_3$ [37] are shown in Figs. 2a and 2b. For both series, a broad band of complex shape with a maximum around 450 nm is observed. The highest luminescence intensity is achieved for the samples with 0.1–0.15 at. % Ce^{3+} in the series of samples obtained using CeO_2 and for the sample with 0.125 at. % Ce^{3+} in the series of samples obtained using $Ce(acac)_3$ (Fig. 2c and 2d). In the spectra of the samples obtained using CeO_2, a pronounced Ce^{3+} $d \rightarrow f$-luminescence band with a maximum around 450 nm is observed at a Ce^{3+} content of 0.1–0.2 at. %. At the same time, for the samples obtained using CeO_2 having Ce^{3+} content less than 0.1 at. %, the PCL spectra are similar to those of the series samples obtained using Eu_2O_3 and $Eu(acac)_3$, with Eu^{2+} content less than 0.1 at. %. This means that the luminescence centers in all these samples are of the same nature.

In general, the highest PCL intensity is observed for Eu^{2+}-doped samples, in particular, at a Eu^{2+} content of 0.5 at. %. The PCL intensity of Ce^{3+} doped samples is significantly lower (up to an order of magnitude). The use of oxides as a source of REM ions gives better results as compared to the use of the corresponding acetylacetonate complexes.

It should be noted that Ce^{3+} is rarely used as an independent luminescence activator in oxynitride matrices; however it is much more often used as a

[1] https://www.castep.org/. Accessed June 11, 2025.

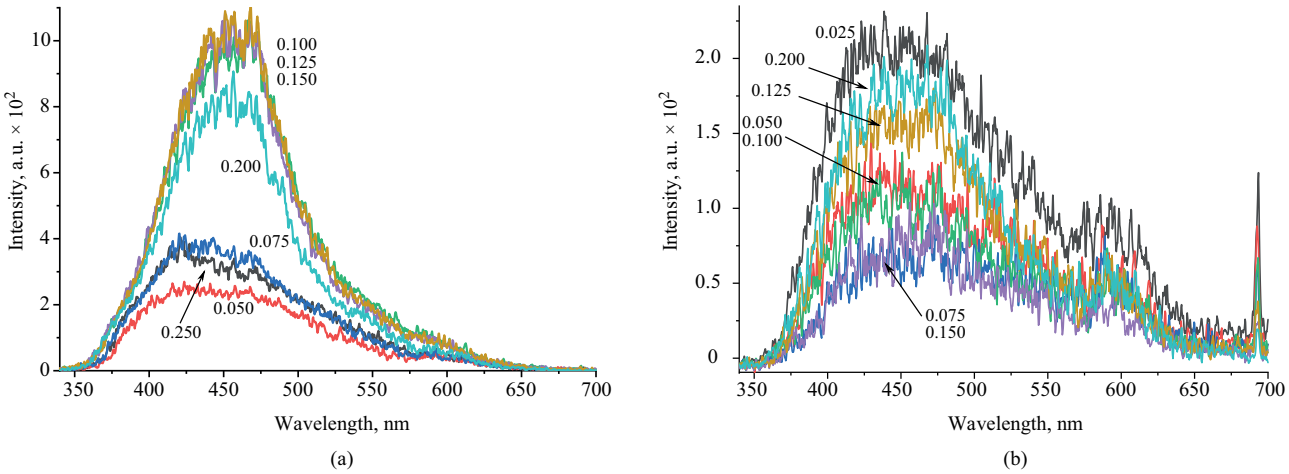

Fig. 2. PCL spectra of Ce^{3+}-doped AlONs prepared with CeO_2 (a) and $Ce(acac)_3$ (b). The concentration in at. % of Ce ions is shown near the curves (reprinted from [37])

sensitizer, primarily for Eu^{2+} and Tb^{3+} ions (see below). Photoluminescent and radioluminescent properties of AlON doped with Ce^{3+} ions are described in [46]. AlON, whose composition is described by the authors as $AlO_{0.86}N_{0.43}$:Ce_x, where $x = 0.005$, 0.01, was obtained by firing mixtures of Al_2O_3 and AlN with the addition of Y_2O_3 as a sintering additive and CeO_2 in a nitrogen current at 1780°C for 2 h. Transparent samples were obtained by cold isostatic pressing of the obtained powder followed by sintering at 1900°C. The excitation spectra of the samples show an PL absorption band with a maximum around 325 nm and the emission spectra show a band with a maximum around 405 nm. Ionization scintillation in the obtained samples was confirmed using a ^{137}Cs (661 keV) radiation source; however, the large width of the forbidden zone and insufficient Ce^{3+} concentration, according to the authors, lead to a low light output. In general, the obtained results confirm the low efficiency of Ce^{3+} ions as luminescence activators in AlON. The actual composition of aluminum oxynitride is not clear from the work, since the composition of $AlO_{0.86}N_{0.43}$ does not correspond to either γ-AlON or one of the other phases described in the pseudo-binary system AlN–Al_2O_3. Moreover, the claimed composition does not correspond to the given loadings of initial components either.

Active studies into the luminescent properties of AlONs doped with Tb^{3+} ions have been focused on obtaining phosphors with luminescence in the green region of the spectrum. Being an effective luminescence activator, Tb^{3+} is most often used in pair with some sensitizer, typically Ce^{3+}. The reason is the high cost of terbium, which, in many cases, makes its independent use economically unfeasible. Thus, [47] studied the properties of AlONs doped with Tb^{3+} (as well as co-doped with Tb^{3+} and Ce^{3+}) prepared by reductive nitriding of mixtures of Al_2O_3, CeO_2, and Tb_4O_7 oxides and aluminum nitride AlN. The authors found that in AlON:Ce^{3+} samples the concentration quenching of photoluminescence starts at Ce^{3+} concentration above 1 at. %, while for Tb^{3+} the critical concentration is 0.5 at. %. In the absorption spectra of AlON:Tb^{3+}, two main bands at 270 and 300 nm are observed, corresponding to the spin-resolved transition $4f^8 \rightarrow 4f^7 5d^1$ in the Tb^{3+} ion. There are 4 narrow intense bands in the emission spectrum corresponding to the transitions from the $^5D_4$ level to the $^7F_6$ (485 nm), $^7F_5$ (543 nm), $^7F_4$ (580 nm), and $^7F_3$ (619 nm) levels in the Tb^{3+} ion.

We also synthesized AlONs doped with ions Tb^{3+} [38]. Samples with Tb^{3+} content from 0.025 to 0.5 at. % relative to aluminum were obtained by two-hour roasting in a nitrogen current of mixtures of amorphous highly dispersed Al_2O_3, AlN, and Tb_2O_3. The study of the phase composition of the obtained samples showed that AlON is the main phase in all cases. In samples with Tb^{3+} content of 0.025, 0.1, and 0.5 at. %, a nitrogen-enriched AlON phase of $Al_7O_3N_5$ composition is identified (in insignificant amounts). At Tb^{3+} content of 0.1 at. % and more, the formation of impurity quantities of phases of corresponding perovskite $TbAlO_3$ and garnet $Tb_3Al_5O_{12}$ aluminates is noted.

The PCL and PL spectra of the obtained AlON samples doped with Tb^{3+} ions with terbium content from 0.025 to 0.5 at. % are presented in Fig. 3. At a Tb^{3+} content of 0.025 at. %, two broad bands with maxima around 400 and 595 nm are observed in the Fourier-transform infrared spectra, which can be attributed to the luminescence of defects in the impurity phase of AlN [41]. In other samples, the AlN content is lower

(or it is not identified at all), and the described bands are not detected in the PCL spectra.

In the PCL spectra of all other AlON:Tb^{3+} samples, a series of bands corresponding to the intra-center electronic $f \rightarrow f$ transitions in Tb^{3+} ions are observed, having maxima around 380, 415, 438, 457, 488, 541, 586, and 621 nm. In particular, the bands with maxima around 488, 541, 586, and 621 nm correspond to $^5D_4 \rightarrow {}^7F_J$ transitions, J = 6, 5, 4, and 3, respectively, while the bands with maxima around 380, 415, 438, and 457 nm correspond to $^5D_3 \rightarrow {}^7F_J$ transitions, J = 6, 5, 4, and 3 [48, 49]. The band with a maximum at about 541 nm corresponding to the $^5D_4 \rightarrow {}^7F_5$ transition has the highest intensity in the PCL spectra, while the band with a maximum at about 457 nm corresponding to the $^5D_3 \rightarrow {}^7F_3$ transition is extremely weakly expressed. The maximum integrated luminescence intensity of AlON:Tb^{3+} samples is achieved at a Tb^{3+} ion concentration of 0.2–0.4 at. %.

The PL emission spectra of AlON:Tb^{3+} samples show all the bands recorded in the PCL spectra (Figs. 3b and 3c), as well as an additional unresolved PCL band having a maximum around 470 nm, which can be attributed to the $^4D_5 \rightarrow {}^7F_5$ transition. The PL excitation spectra (PLE) reveal a number of bands with maxima around 220, 230, 260, and 285 nm, which can be attributed to the $4f^8 \rightarrow 4f^7 5d^1$ transitions in Tb^{3+} ions.

In the PL emission spectra, the probabilities of the $^5D_4 \rightarrow {}^7F_J$ and $^5D_3 \rightarrow {}^7F_J$ electronic transitions differ as a function of the excitation wavelength (Fig. 3b, curves *1* and *2*). The PLE spectra also behave in a similar way. When the PLE spectra are recorded for the 543 and 415 nm bands, the profile of the spectra changes. The band

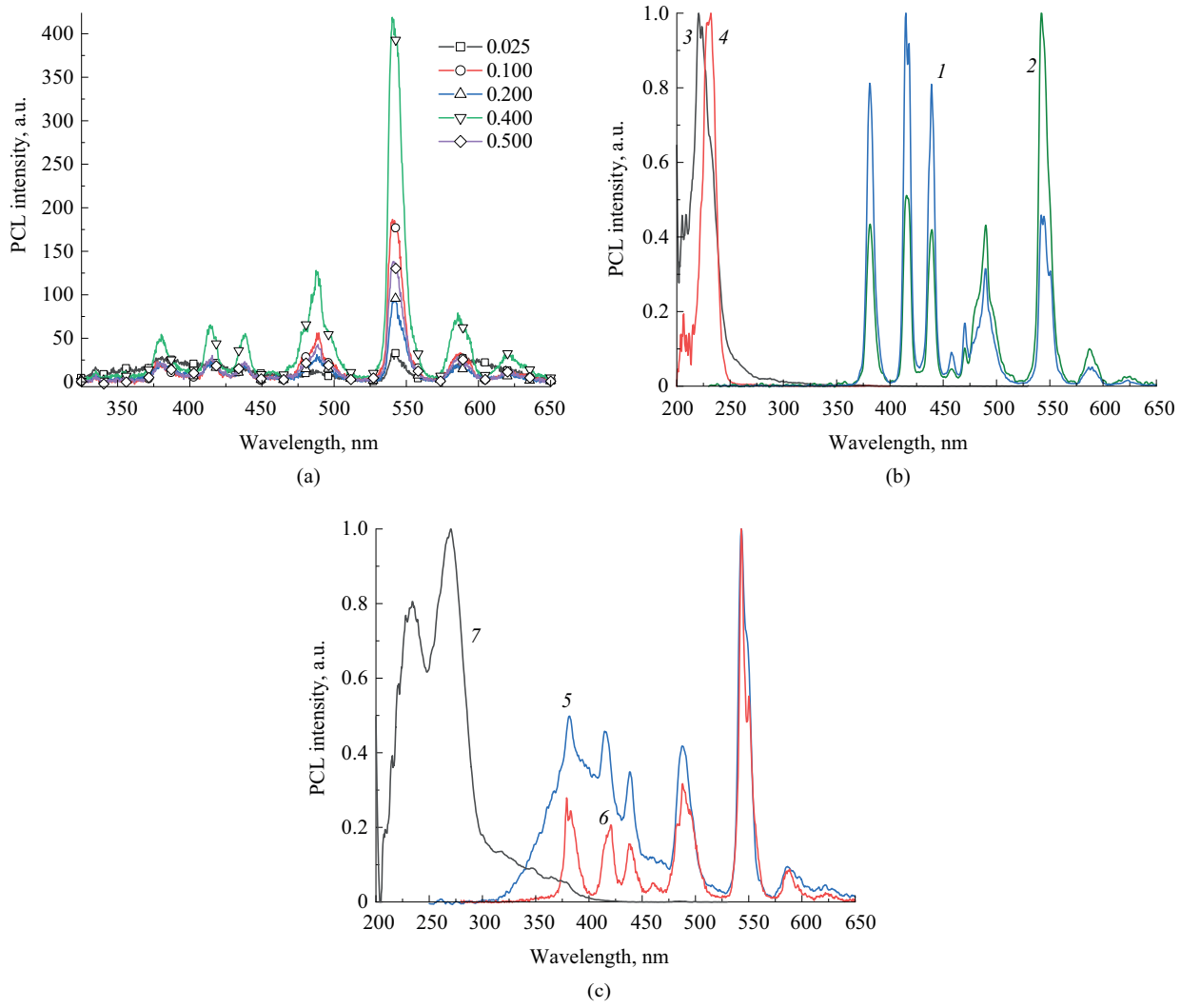

Fig. 3. (a) PCL emission spectra of $Al_5O_6N:Tb^{3+}$ samples with a Tb^{3+} content ranging from 0.025 at. % to 0.5 at. %; (b) photoluminescence (PL) and photoluminescence excitation (PLE) spectra of an $Al_5O_6N:Tb^{3+}$ sample with a Tb^{3+} content of 0.1 at. % (*1* and *2* are the PL spectra upon excitation at 231 and 220 nm; *3* and *4* are the PLE spectra for luminescence bands at 543 and 415 nm); (c) PL and PLE spectra of an $Al_5O_6N:Tb^{3+}$ sample with a Tb^{3+} content of 0.4 at. % (*5* and *6* are the PL spectra upon excitation at 233 and 270 nm; *7* is the PLE spectrum for the luminescence band at 543 nm) (reprinted from [38])

with a maximum around 220 nm becomes dominant in the PLE spectra for the $^5D_4 \rightarrow {}^7F_J$ transitions, while for the $^5D_3 \rightarrow {}^7F_J$ transitions the band has a maximum around 230 nm (Fig. 3b, curves *3* and *4*).

The PL and PLE spectra of samples with high Tb^{3+} content have some differences. Thus, the PLE spectrum of the AlON:0.4 at.% Tb sample (Fig. 3c, curve *7*) is also caused by the $4f^8 \rightarrow 4f^7 5d^1$ transition (spin-allowed transition $^7F_6 \rightarrow {}^7D_J$) in Tb^{3+} ions, but differs by the presence of an intense excitation band with a maximum around 270 nm, which is related to the spin-allowed transition $^7F_6 \rightarrow {}^9D_J$, and a broad structureless region in the range of 300–400 nm. The narrow bands in the PL spectra of AlON:0.4 at. % Tb are also due to the $^5D_4 \rightarrow {}^7F_J$ and $^5D_3 \rightarrow {}^7F_J$ transitions in Tb^{3+} ions. The broad band with a maximum near 400 nm may belong to the intrinsic luminescence of AlON or the luminescence of the AlN impurity [50], which begin to be effectively excited below 250 nm. The above-mentioned differences in the PL and PLE spectra of AlON:Tb^{3+} samples with low and high content of Tb^{3+} ions can be related to the effect of cross-relaxation of electronic excitations ($^5D_3$,$^7F_6 \rightarrow {}^5D_4$,$^7F_0$) [48, 50] between nearby Tb^{3+} ions in the AlON matrix.

Ions of other rare earth metals have not generally been used as dopants for aluminum oxynitrides until recently. In 2009–2012, a team of authors from the Shanghai Institute of Ceramics described the ap-conversion of infrared (IR) radiation at 980 nm in AlON doped with Er^{3+} ions with addition of Mg^{2+} [51, 52]. AlONs with Er^{3+} content up to 3.0 mol % were studied. The obtained samples showed intense green and red luminescence with maxima in the PL spectra around 548 and 666 nm, which are the result of $^4S_{3/2}/^2H_{11/2} \rightarrow {}^4I_{15/2}$ and $^4F_{9/2} \rightarrow {}^4I_{15/2}$ transitions, respectively. By varying the doping concentration of Er^{3+} ions, the predominant color of the phosphors can be tuned due to the cross relaxation like $^4F_{7/2} \rightarrow {}^4F_{9/2}$ and $^4F_{9/2} \leftarrow {}^4I_{11/2}$. Upon co-doping with Er^{3+}, Mg^{2+}, broadening of the bands in the PL spectra was observed [51]. According to X-ray phase analysis (XRD) data, the solubility of Er^{3+} ions in the AlON matrix increased with the addition of Mg^{2+}, and band broadening was observed in the PL spectra. The intensity of the red emission band increased with increasing Mg^{2+} content up to 0.6 mol %, and decreased with further addition of Mg^{2+}. The authors propose that the introduction of Mg^{2+} up to a certain limit facilitates the introduction of Er^{3+} into the AlON lattice and lowers its symmetry due to the formation of oxygen vacancies, leading to the enhancement of red emission due to energy transfer. When the critical concentration of Mg^{2+} is reached, the effect of luminescence quenching on the formed defects begins to prevail.

AlONs doped only with Er^{3+} ions were obtained in [53]. The authors noted the dual role of erbium as a sintering additive (in the form of Er_2O_3) and a fluorescence activator. Upon excitation with 980 nm radiation, the previously described green and red bands, as well as a band with a maximum around 845 nm corresponding to the transition $^4S_{3/2}/^2H_{11/2} \rightarrow {}^4I_{13/2}$, were observed in the PL spectra. In the IR emission spectra of AlON:Er^{3+}, an intense band with a maximum at 1534 nm corresponding to the $^4I_{13/2} \rightarrow {}^4I_{15/2}$ transition due to the radiation-free $^4I_{11/2} \rightarrow {}^4I_{13/2}$ transition and AP-conversion emission at 845 nm was observed.

The study of AlONs doped with ions of a wide range of REMs, including Sc, La, Pr, Sm, Sm, Gd, Dy, Er, and Yb, was performed several years ago at Yeungnam University (Republic of Korea). All the above elements were used in the form of the corresponding nitrates as well as oxides as sintering additives to obtain transparent AlONs [54]. The authors used the ratio Al_2O_3:AlN = 9:2.503 instead of 9:5 to increase sinterability by creating additional cation vacancies, metals were introduced in the amount of 0.2 wt %. Two-stage sintering under nitrogen pressure up to 2 atm at temperatures of 1610–1650°C and 1940°C allowed obtaining single-phase samples γ-AlON. The highest efficiency was demonstrated by Pr in the form of nitrate. Unfortunately, no measurements of optical properties were made by the authors, but relatively recently the same team studied the photoluminescent properties of AlON samples doped with Sm and Yb ions, albeit to a very limited extent [55]. In the PL excitation spectra of AlON:Sm^{3+}, a main band with a maximum around 340 nm was observed, which is due to the $4f^6 \rightarrow 4f^5 5d^1$ transition, while in the emission spectra, narrow bands with maxima around 690 (main band), 700, and 730 nm appear corresponding to the $^5D_0 \rightarrow {}^7F_J$ transitions, where J = 0.1 and 2, respectively. In the PL excitation spectra of AlON:Yb^{3+} there is one band with a maximum at about 333 nm, due to the $^1S_0 \rightarrow {}^7F_{7/2}T_{2g}$ transition, to which corresponds a band in the emission spectrum with a maximum at about 435 nm, arising from the reverse transition. Thus, AlON:Sm^{3+} phosphors belong to red light phosphors, while those of AlON:Yb^{3+} correspond to blue light phosphors.

The doping of oxynitride materials with two REM ions simultaneously has recently attracted increasing interest. If the material is doped with two different REM ions, one of them plays the role of an activator providing light emission, while the other plays the role of a sensitizer promoting absorption of excitation light. Efficient energy transfer between the two types of metal ions is also important for the sensitizing effect. Typically, energy transfer occurs through dipole-dipole or dipole-quadrupole interactions. The Eu^{2+}/Ce^{3+} pair is often used for co-doping nitride materials due to the emission

band of Ce^{3+} overlapping sufficiently with the excitation band of Eu^{2+}. For example, $SrSi_2O_2N_2$ doped with Eu^{2+} and Ce^{3+} ions ($SrSi_2O_2N_2$:xEu^{2+},yCe^{3+}; x = 0–0.04, y = 0–0.04) exhibits green-yellow luminescence in the PL spectra with a maximum around 540 nm [56, 57].

We have obtained samples of AlONs doped with Eu^{2+} and Ce^{3+} ions of the composition AlON:xEu^{2+},yCe^{3+}; x = 0.25: y = 0.01, 0.025, 0.04, and 0.08; y = 0.025: x = 0.1, 0.25, 0.4, and 0.8 [39]. The main phase of the samples, which are almost single phase, can be described as Al_5O_6N; trace amounts of α-Al_2O_3 and AlN are also present. A broad non-elemental band is observed in the PCL spectra (Figs. 4a and 4b). The band maximum is located at ~405 nm with a shoulder in the range of 450–550 nm. The band is approximated by two bands—a narrower band with a maximum around 401 nm, which corresponds to the $5d\rightarrow4f$ transitions in Ce^{3+} ions, and a broader band with a maximum around 447 nm, which corresponds to the $5d\rightarrow4f$ transitions in Eu^{2+} ions.

The position of the band maximum in the PCL spectra depends weakly on the Eu^{2+} ion content, while the integrated luminescence intensity varies with the Eu^{2+} and Ce^{3+} content. At an Eu^{2+} content of 0.25 at. %, the highest intensity is observed at a Ce^{3+} content of 0.04 at. %. On the other hand, at a fixed Ce^{3+} content of 0.025 at. %, the highest intensity is observed at an Eu^{2+} content of 0.1 at. %. An increase in Eu^{2+} content leads to a decrease in the intensity of both Eu^{2+} and Ce^{3+} bands. Conversely, increasing the Ce^{3+} content decreases the intensity of Eu^{2+} band and increases the intensity of

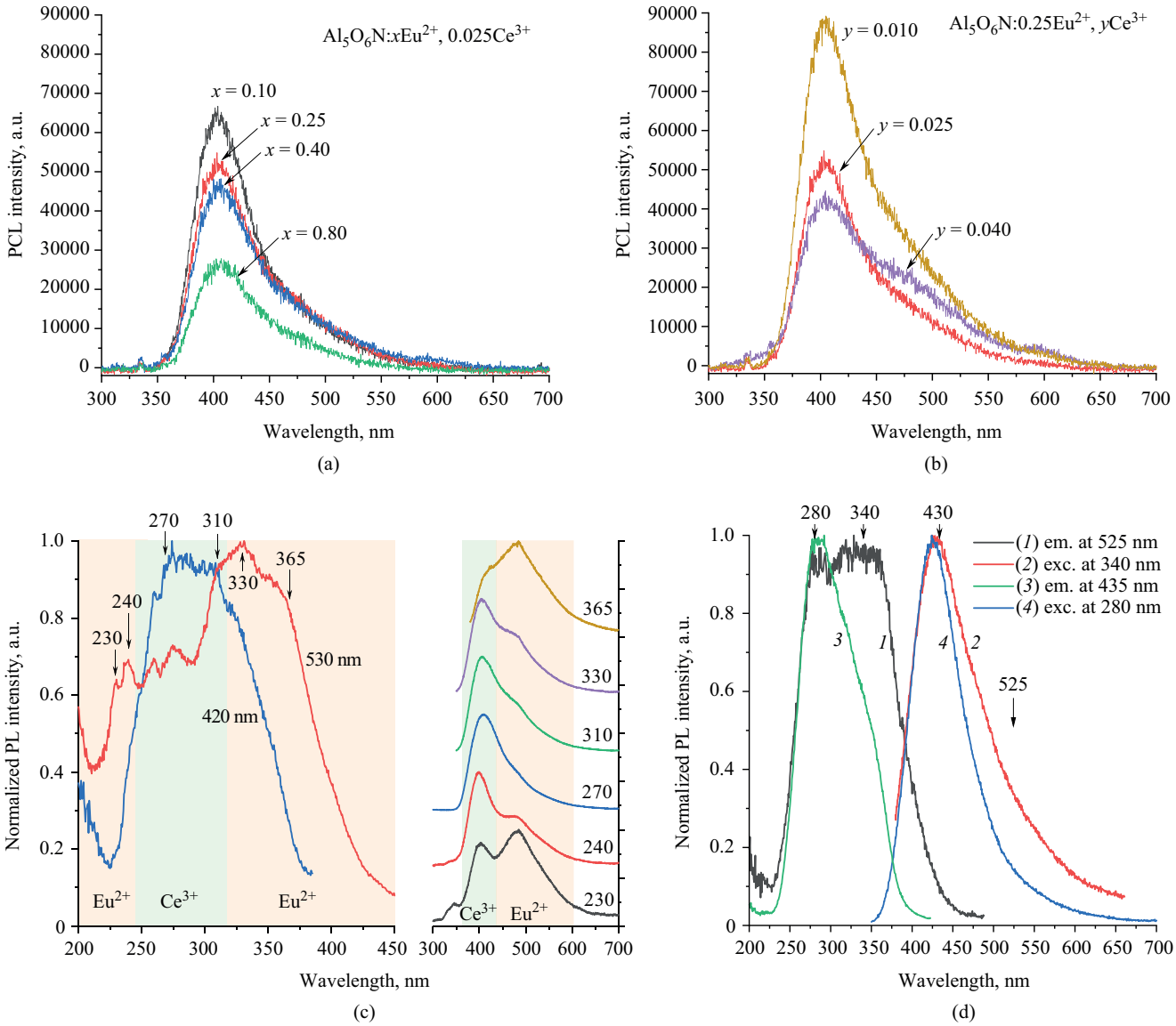

Fig. 4. (a) PCL spectra of samples Al_5O_6N:xEu^{2+},yCe^{3+}: x = 0.1, 0.25, 0.4, 0.8; y = 0.025; (b) PCL spectra of samples Al_5O_6N:xEu^{2+},yCe^{3+}: x = 0.25; y = 0.01, 0.025, 0.04; (c) PLE and PL spectra of Al_5O_6N:0.25Eu^{2+},0.01Ce^{3+} sample; (d) PL and PLE spectra of Al_5O_6N:0.25Eu^{2+},0.04Ce^{3+} sample (reprinted from [39])

Ce^{3+} band, thus also increasing the total luminescence intensity.

Three bands distinguished in the PLE spectra (Fig. 4c) correspond to the excitation of different bands of the PL spectra (Fig. 4d). The ~405 nm PL band is effectively excited in the range of 245–320 nm. The broad band with a maximum of 455 nm is more efficiently excited below 245 nm, as well as in the range of 320–450 nm. The shape of the PLE spectra of the sample with Ce^{3+} content of 0.04 at. % differs from the samples with Ce^{3+} content of 0.01 at. %. The relative intensities of the excitation band at 280 nm and the PL band at 405 nm are maximal for $Al_5O_6N:0.25Eu^{2+},0.04Ce^{3+}$. Analysis of the PL and PLE spectra allows us to conclude that the observed bands belong to the $5d\rightarrow4f$ transitions in Eu^{2+} and Ce^{3+} ions. This is confirmed by earlier results for AlONs doped with REM ions of the same species [35, 37, 58–60]. However, the maximum of the Ce^{3+} excitation band in the samples obtained by us is shifted compared to that for the band in the Ce^{3+} spectrum presented in [60] due to the possible energy transfer $Ce^{3+}\rightarrow Eu^{2+}$. Thus, in this case, a sensitizing effect of Ce^{3+} with respect to Eu^{2+} is observed. Presumably, the main energy transfer pathway is the radiation-free dipole-dipole interaction, possibly with some contribution from dipole-quadrupole interactions.

More recently, a series of blue-light phosphors γ-AlON:yCe^{3+},xEu^{2+} (y = 0–0.025, x = 0–0.01) were prepared in a similar way and their photoluminescence was studied [61]. The effect of sensitization of Eu^{2+} ions by Ce^{3+} ions was also demonstrated for them; the energy transfer from Ce^{3+} to Eu^{2+} is confirmed by a significant overlap between the emission spectrum of γ-AlON:$0.025Ce^{3+}$ (λ_{ex} = 285 nm) and the excitation spectrum of γ-AlON:$0.004Eu^{2+}$ (λ_{em} = 400 nm). As described above, the energy transfer is mainly due to radiation-free dipole-dipole interactions. The critical energy transfer distance was determined as 25.45 Å from concentration quenching of luminescence. The presented results showed that γ-AlON:Eu^{2+},Ce^{3+} phosphors can be considered as promising candidates for the role of the blue component in full-spectrum warm WLEDs.

Ce^{3+} is also quite frequently used as a sensitizer for Tb^{3+}. In [59], the phosphor $Al_5O_6N:0.5\%Ce^{3+},0.67\%Tb^{3+}$ was obtained by nitriding cinders prepared from nitrates of the corresponding metals. In its PL emission spectrum obtained under excitation with light at 275 nm, 4 main bands with maxima around 485, 540, 580, and 625 nm were observed, which correspond to $^5D_4\rightarrow{}^7F_J$ transitions in Tb^{3+} ions, where J = 6, 5, 4, and 3, respectively. The intensity of the band with a maximum around 540 nm for the $Al_5O_6N:0.5\%Ce^{3+},0.67\%Tb^{3+}$ sample was found to be 10 times higher than that for the $Al_5O_6N:0.67\%Tb^{3+}$ sample. Increasing the Tb^{3+} content to 1 mol % did not lead to an increase in the intensity of the bands in the emission spectrum; moreover, at a Tb^{3+} content of 3 mol %, it decreased by a factor of five. Thus, Ce^{3+} has been shown to be an effective sensitizer for Tb^{3+}. The main mechanism of energy transfer seems to be dipole-dipole interactions.

Similar results were obtained in [47]. Additionally, it was shown that the energy transfer efficiency exceeds 98% at a Tb^{3+} content of 3 mol %, although concentration quenching leads to a decrease in the overall emission.

Tb^{3+} can also be sensitized by Eu^{2+}, such as in $Al_5O_6N:0{,}2Eu^{2+},xTb^{3+}$ (x = 0–0.5) [62]. Although the energy transfer efficiency did not exceed 25%, the reason for this was most likely due to the low total dopant ion content. The main mechanism of energy transfer is radiation-free dipole-dipole interactions at a critical transfer distance of 6.49 Å. The materials are green light phosphors, whose PL emission spectra obtained under excitation with light at 330 nm are the sum of spectra due to Eu^{2+} and Tb^{3+} ions.

We also studied the PL and PCL spectra of AlON:xTb^{3+},yCe^{3+} samples (x = 0.4%, y = 0.01–0.08%), which were prepared by a similar AlON:xEu^{2+},yCe^{3+} method [39]. According to XRD data, all samples contain Al_5O_6N as the major phase; the minor phases present in impurity amounts are represented by some other AlON polymorphs ($Al_8O_3N_6$, $Al_{11}O_{15}N$, etc.). Terbium and cerium aluminates were not detected.

The PCL and PLE/PL spectra of $Al_5O_6N:x$Tb^{3+},yCe^{3+} samples are shown in Fig. 5. The emission spectra show narrow bands with maxima around 380, 415, 439, 460, 472, 485, 540, 582, and 620 nm, which correspond to the in-center $f\rightarrow f$ transitions in Tb^{3+} ions. As in the case of AlONs doped only with Tb^{3+} ions [38], the bands with maxima around 485, 540, 582, and 620 nm correspond to $^5D_4\rightarrow{}^7F_J$ transitions, J = 6, 5, 4, 4, and 3, while the 380, 415, 439, 460, and 472 nm bands correspond to $^5D_3\rightarrow{}^7F_J$ transitions, J = 6, 5, 4, 3, and 2 [48, 49]. The high intensity band of $^5D_3\rightarrow{}^7F_J$ transitions is observed in the PL spectra only under selective excitation as has been shown earlier for $Al_5O_6N:Tb^{3+}$ phosphors [38]. The $^5D_4\rightarrow{}^7F_5$ transition band at 542 nm has the highest intensity in the PCL spectra. Broad bands of $d\rightarrow f$ transitions in Ce^{3+} ions were not observed. Increasing the Ce^{3+} content leads to an increase in the integrated intensity of the bands related to Tb^{3+}. The totality of these facts clearly indicates an effective radiation-free energy transfer from Ce^{3+} to Tb^{3+}.

AlON:xTb^{3+},yEu^{2+} (x = 0.4%, y = 0.1–0.8%) samples were also obtained. As in all other cases, no reduction of Tb^{3+} was observed at complete reduction of Eu^{3+} to Eu^{2+}. All AlON:xTb^{3+},yEu^{2+} samples contain Al_5O_6N as the main phase and corundum as an impurity. In addition, some amount of $EuAl_{12}O_{19}$ phase is present in

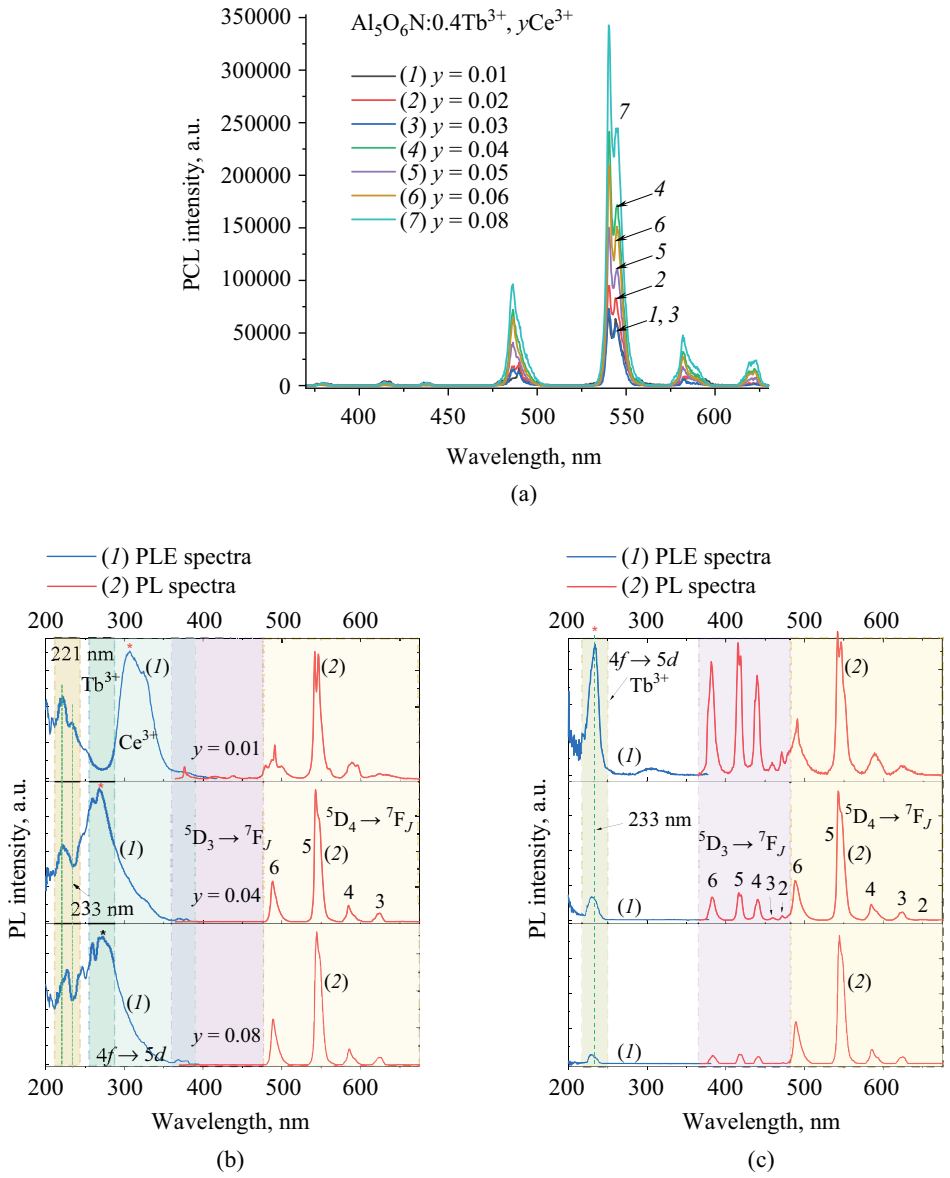

Fig. 5. (a) PCL spectra of Al_5O_6N:xTb^{3+},yCe^{3+} samples; PLE (b) and PL (c) spectra of Al_5O_6N:xTb^{3+},yCe^{3+} samples (reprinted from [39])

the AlON:xTb^{3+},yEu^{2+} samples, indicating incomplete dissolution of Eu^{2+} in the AlON matrix.

The PCL spectra of Al_5O_6N:xTb^{3+},yEu^{2+} are presented in Fig. 6. The observed narrow bands, which have maxima around 415, 437, 485, 540, 582, and 620 nm, are associated with the intra-center f→f transitions in Tb^{3+} ions as described above. The band with a maximum around 380 nm observed for the AlON:Tb^{3+}/Ce^{3+} samples is not represented here due to overlap with a broad asymmetric band with a maximum around 410 nm and a half-width of 66 nm, which is associated with d→f transitions in Eu^{2+}. The integrated luminescence intensity due to Tb^{3+} ions depends very weakly on the Eu^{2+} concentration. At the same time, concentration quenching of Eu^{2+} luminescence is observed; the maximum intensity is reached at Eu^{2+} content of 0.3 at. %.

The PL and PLE spectra recorded in the fluorescence mode mainly consist of broad bands that are related to the 4f↔5d transitions in Eu^{2+} (Fig. 6b). The band in the PLE spectra is the sum of two bands with maxima around 260 and 300 nm. Two broad bands with maxima around 395 and 455 nm are observed in the PL spectra. The PL spectra recorded in the phosphorescence mode (Fig. 6c) consist of narrow bands associated with f→f transitions in Tb^{3+} as described above. The broad bands attributed to Eu^{2+} are not observed. The broad band in the range of 250–400 nm PLE in the phosphorescence spectra, which is attributed to the 4f→5d transitions in Eu^{2+}, clearly indicate the energy transfer of Eu^{2+}→Tb^{3+},

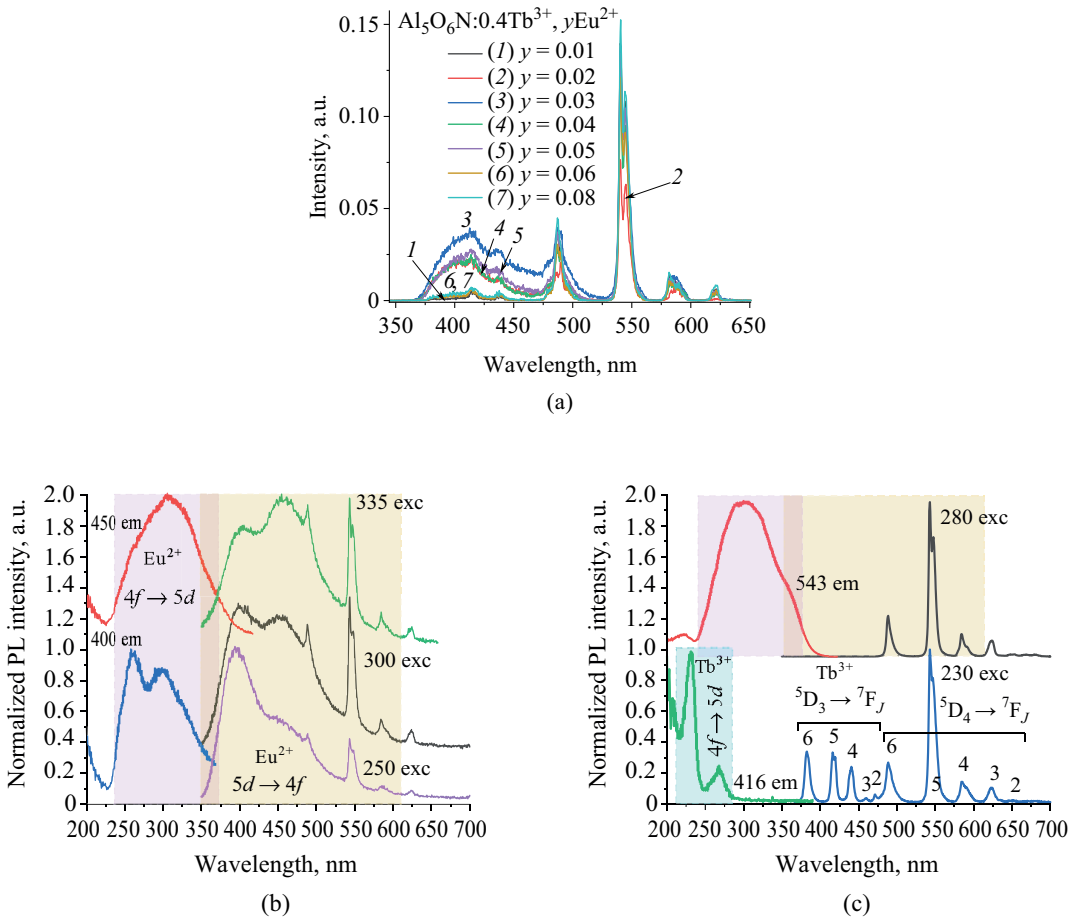

Fig. 6. (a) PCL spectra of samples $Al_5O_6N:0.4Tb^{3+},yEu^{2+}$; PL and PLE spectra for $Al_5O_6N:0.4Tb^{3+}/0.3Eu^{2+}$ sample recorded in fluorescence (b) and phosphorescence (c) modes (reprinted from [39])

albeit at a reduced transfer efficiency. The probable reason for this is that the total concentration of Tb^{3+} and Eu^{2+} ions exceeds the concentration limit of quenching in contrast to the $Al_5O_6N:Tb^{3+},Ce^{3+}$ samples.

Concluding this section, it should be noted that the developed method allows easy and reproducible preparation of AlONs doped with both one and two different types of REM ions, which can be used as luminophores. The obtained materials exhibit intense cathodo- and photoluminescence over a wide wavelength range, which can be tuned by varying the dopant or dopant ions as well as their content in the AlON matrix. Sensitization and concentration quenching effects are observed for the obtained samples, which should be taken into account when selecting the optimal composition for particular applications.

Aluminum oxynitrides doped with TM ions

Until recently, data on aluminum oxynitride-based systems containing TM ions were very limited. The exception was AlONs doped with manganese ions [31, 63–66], which are green light phosphors having a narrow emission band. A characteristic view of the PLE and PL spectra of γ-AlON:xMn^{2+} (x = 0.03–0.15) samples obtained by firing of Al_2O_3, AlN, and $MnCO_3$ mixtures with the addition of oxides or carbonates of alkaline earth and alkali metals for charge compensation is presented in [31]. The spectral characteristics of all samples are very similar except for the fluorescence intensity. The PLE spectrum (λ_{em} = 510 nm) consists of several bands with maxima at 340, 360, 380, 424, and 445 nm [31], which correspond to transitions from the main level $^6A_1$ to the $^4T_2(^4P)$, $^4E(^4G)$, $^4T_2[^4E(^4G)$, $^4A(^4G)]$, and $^4T_2(^4G)$ levels, respectively. Since all these transitions are spin- and parity forbidden, the intensities of the corresponding bands in the PLE and PL spectra are also reduced. The PL spectrum shows a narrow band with a maximum at 510 nm (λ_{ex} = 445). The narrow band in the green region of the spectrum is characteristic of the Mn^{2+} ion due to the $^4T_1(^4G)\rightarrow{}^6A_1$ transition. Furthermore, the intensities of the bands in the PL spectrum monotonically increase with increasing Mn^{2+} content to reach a maximum at x = 0.07, after

which concentration quenching of luminescence is observed. In general, the distance between Mn^{2+} ions decreases with increasing x, which leads to a decrease in the radiative transition rate and an increase in the rate of non-radiative transitions due to cross-relaxation. The calculated critical distance between manganese ions was 8.3 Å, which is significantly larger than the distance allowing exchange interactions (5 Å). Analysis of the dependence of lg I/x on lg x (where I is the luminescence intensity, x is the activator content) showed that the most probable mechanism of energy transfer is dipole-dipole interactions.

The first report on Cr^{3+}-doped AlONs appeared in 2020 in [67]. Powders γ-AlON:Cr^{3+} with Cr^{3+} content from 0.25 to 1.25 mol % were obtained by high-temperature roasting of the corresponding oxides and AlN in nitrogen atmosphere. The powders of the obtained materials consist of homogeneous particles of hexagonal shape with the size from 50 to 100 nm. According to XRD data they represent γ-Al_5O_6N, no impurity phases were observed. According to X-ray photoelectron spectroscopy (XPS) data, chromium is present in the form of Cr^{3+} ions in the octahedral environment of oxygen atoms, i.e., it either replaces aluminum in the corresponding positions or occupies $V_{Al}O_6$ vacancies. Two broad intense bands with maxima around 430 and 588 nm are observed in the PLE spectra, which can be attributed to the $d \rightarrow d$ transitions $^4A_2(^2F) \rightarrow {}^4T_1(^4F)$ and $^4A_2(^2F) \rightarrow {}^4T_2(^4F)$, respectively.

The narrow intense band in the PL emission spectrum (λ_{ex} = 588 nm) with a maximum at 693 nm is attributed to the $^2E(^2G) \rightarrow {}^4A_2(^4F)$) transition, while the broad band with a maximum at 720 nm is presumably due to defects in the AlON matrix.

More recently, we have investigated AlONs doped with titanium [68], cobalt [69], and iron [70] ions. As well as samples of AlONs doped with REM ions, these were prepared by high-temperature roasting of mixtures of amorphous highly dispersed aluminum oxide Al_2O_3 and AlN in a nitrogen current under 1 atm pressure for 2 h at 1750°C. In the case of cobalt, the aluminum oxide was pre-doped using $Co(OAc)_2 \cdot 4H_2O$ [33]. In the case of titanium and iron, the corresponding oxides were added directly to the mixture of Al_2O_3 and AlN. The TM content ranged from 0.01 to 5.0 at. % relative to aluminum.

According to XRD data, all titanium-doped AlN samples are almost pure γ-Al_5O_6N [68]. Samples with 0.05–0.2 at. % of titanium contain AlN (less than 2 vol %) as an impurity. Samples with titanium content of 0.5 at. % and more contain TiN as an impurity, whose content increases with increasing total titanium content. Interestingly, even a sample with 0.05 at. % titanium does not contain corundum as an impurity phase. Typically, to suppress the formation of corundum in the synthesis of γ-AlON, Mg^{2+} ions are incorporated in the amount from 0.5 to 10 at. %. It can be concluded that titanium effectively promotes the formation of the γ-Al_5O_6N phase, having a solubility limit in the AlON matrix ranging from 0.2 to 0.5 at. %. According to the RFES data, titanium ions occupy octahedral positions in the AlON structure to form [TiN_6], [TiO_xN_{6-x}], and [TiO_6] links, which are quantitatively correlated as 39:38:23. Titanium nitride TiN, as measured by Raman spectroscopy, probably forms a thin film on the surface of the AlON particles.

In the absorption spectra in the UV-visible range of AlON:Ti^{3+} samples, which are obtained by the computational method using the Kubelka–Munk expression [71] from diffuse reflectance spectra, an absorption band with a maximum around 255 nm is observed. This is typical for AlON and associated with electronic transitions in defects such as V_{Al} [72]. The presence of a pronounced fundamental absorption edge in the absorption spectra formed a basis for estimating the optical width of the forbidden zone E_g by the Tautz method [73] with subsequent correction of the absorption spectra. It was found that E_g varies from 5.68 to 5.72 eV when the titanium content changes.

The PCL spectra of all samples can be represented by the sum of four luminescence bands with maxima at 393, 483, 602, and 765 nm (Fig. 7). The bands with maxima around 393 and 483 nm probably belong to intrinsic defects of the type of electroneutral complexes [V'''_{Al}–$3O^{\bullet}_N$]. The latter are destroyed by X-ray irradiation and form charged defect states V'''_{Al}, $3O^{\bullet}_N$, [V'''_{Al}–$O^{\bullet}_N$]$^{2-}$ and [V'''_{Al}–$2O^{\bullet}_N$]$^{-}$ [72]. The electronic transitions arising from these defects are manifested by several emission bands in the spectra of non-stoichiometric AlON compounds. However, the nature of intrinsic luminescence in AlON is still debatable. It is interesting to note that the intensity of these bands decreases with increasing titanium content. Apparently, this is due, at least in part, to a decrease in the number of intrinsic defects.

The narrower bands with maxima at 602 and 765 nm can be attributed to defects due to the presence of impurities. Compounds containing Mn^{2+} ions are often found as an uncontrolled impurity in AlN, which causes the appearance of a red luminescence band with a maximum around 600 nm [74]; a small amount of AlN is also determined by XRD in the studied samples. As for the band with a maximum around 765 nm, this can be attributed either to Ti^{3+} ions in the Al_2O_3 matrix [75], whose phase is also defined as impurity, or to Fe^{2+} ions, which can also be active in this part of the spectrum [76, 77].

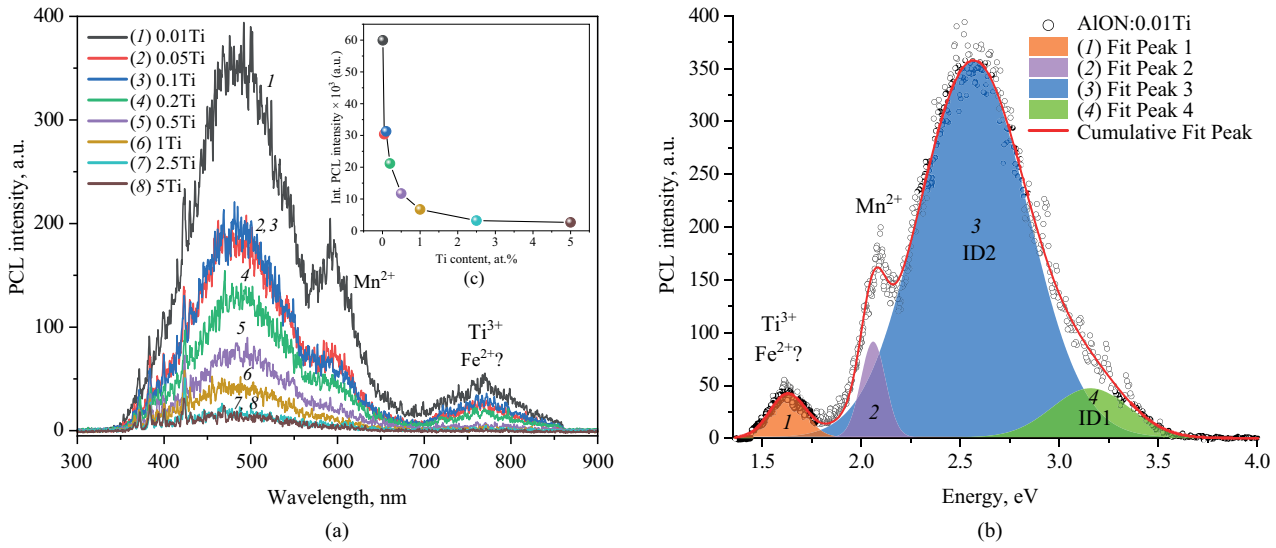

Fig. 7. (a) PCL spectra of the AlON:Ti samples; (b) decomposition of PCL spectrum of AlON:0.01Ti by 4 Gaussian bands; (c) dependence of integral PCL intensity on the total titanium content (reprinted from [68])

The pronounced tendency with increased titanium content to decrease the total luminescence intensity of AlON, as well as each of the bands separately, is probably due to the formation of an increasing amount of TiN on the surface of AlON particles, which has high absorption in the UV- and visible parts of the spectrum [78].

AlON:Co samples were obtained by high-temperature firing of mixtures of amorphous highly dispersed aluminum oxide Al_2O_3 pre-doped with Co ions. $Co(OAc)_2 \cdot 4H_2O$) and AlN in a nitrogen current under 1 atm pressure at 1750°C for 2 h as the starting material [69]. The cobalt content ranged from 0.01 to 5.0 at. % relative to aluminum.

In all AlON:Co samples, the Al_5O_6N phase is the main phase according to XRD data. The samples with cobalt content from 0.01 to 0.5 at. % contain a small admixture of AlN. In samples with cobalt content of 1.0 and 2.5 at. %, a new impurity phase is detected, which becomes the only impurity in the AlON:5.0%Co sample. However, it was not possible to identify this phase. Corundum as an impurity phase was not detected even at the minimum cobalt content (0.01 at. %), as in the case of titanium ion doping.

The study of AlON:Co samples by XRD showed that the spectra of Al 2p and O 1s fully coincide with those of AlON:Ti samples. The spectra of the ground level N 1s show several peaks. The main peak (396.5 eV) appears to correspond to the Al–N bond [79], although this is shifted towards lower bond energies. A similar low-energy shift has been observed previously for numerous systems containing Me–N–O type bonds, such as Ti–N–O [80]. The second peak may be due to the formation of Co–N bonds.

As in the case of AlON:Ti, the optical bandgap width in AlON:Co samples was estimated by the Tautz method with subsequent correction of the absorption spectra. The E_g value varied from 5.72 to 5.84 eV when the cobalt content was varied.

The PCL spectra of the prepared AlON:Co samples are shown in Fig. 8. Three broad luminescence bands with maxima around 476, 595–600, and 750–760 nm are observed for all the samples. The AlON:0.05%Co sample exhibits the brightest luminescence. With increasing cobalt concentration, the intensity of all the bands decreases. The band with a maximum around 480–500 nm can be attributed to defects in the $[V'''_{Al}–3O^{\bullet}_{N}]$ type structure, and the bands with maxima around 600 and 765 nm to impurity emission centers of Mn^{2+} and Ti^{3+} or Fe^{2+}, respectively, as in the case of titanium-doped samples [68, 72].

AlON:Fe^{3+} samples were obtained by high-temperature roasting of mixtures of amorphous highly dispersed aluminum oxide Al_2O_3, AlN, and Fe_2O_3 in a nitrogen current under a pressure of 1 atm for 2 h at a temperature of 1750°C [70]. The Fe^{3+} content ranged from 0.01 to 5.0 at. % relative to aluminum. The diffractograms of the obtained samples show that the main reflections correspond to the Al_5O_6N phase with a small admixture of AlN. Besides AlN, an additional phase was present in all samples, which could not be identified. The total content of AlN and unidentified phase did not exceed 5 vol %. As in the case of doping with Ti and Co ions, the minimum iron content (0.01 at. %) already allows the formation of the α-Al_2O_3 phase to be suppressed.

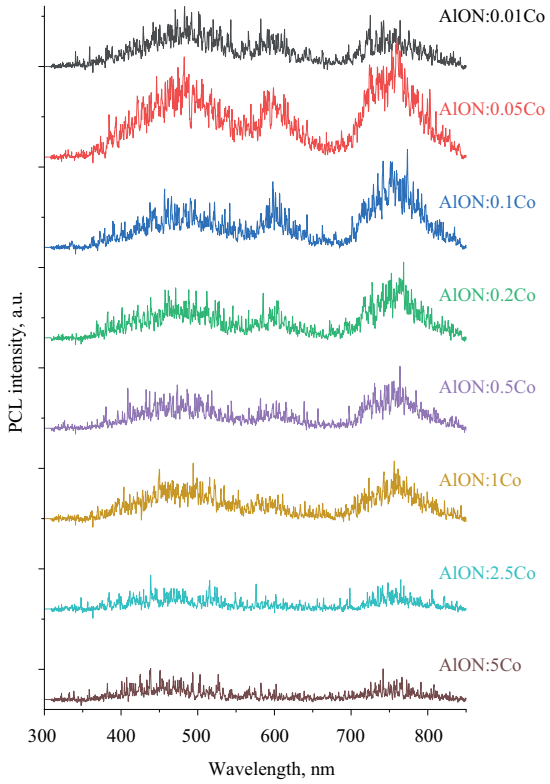

Fig. 8. PCL spectra of AlON:*x*%Co, *x* = 0.01–5.00 (reprinted from [69])

The optical bandgap width in AlON:Fe samples as evaluated by the Tautz method with correction of absorption spectra showed values in the range of 5.76–5.88 eV. The PCL spectra of AlON:Fe^{3+} samples (Fig. 9) contain broad luminescence bands with maxima around 495, 595, and 760 nm. The sample with the minimum iron content, AlON:0.01%Fe, has the most intense emission. The PCL spectra can be approximated by four bands with maxima around 398, 492, 602, and 738 nm. The band with maximum around 398 nm refers to radiative transitions in AlN [72]. The band with maximum around 492 nm is a consequence of emission of defects of the [V'''_{Al}–$3O^{\bullet}_{N}$] type. The bands with maxima around 602 and 738 nm appear to be related to the emission of impurity ions (possibly Mn^{2+} and others).

The results of the studies of AlONs doped with TM ions allowed us to determine the state of TM ions in AlON matrices along with the solubility limits, as well as the influence of the nature and concentration of TM on the optical bandwidth and luminescent properties, which in the case of AlON:Ti, AlON:Co, and AlON:Fe are determined, first of all, by defects in the intrinsic structure of the AlONs.

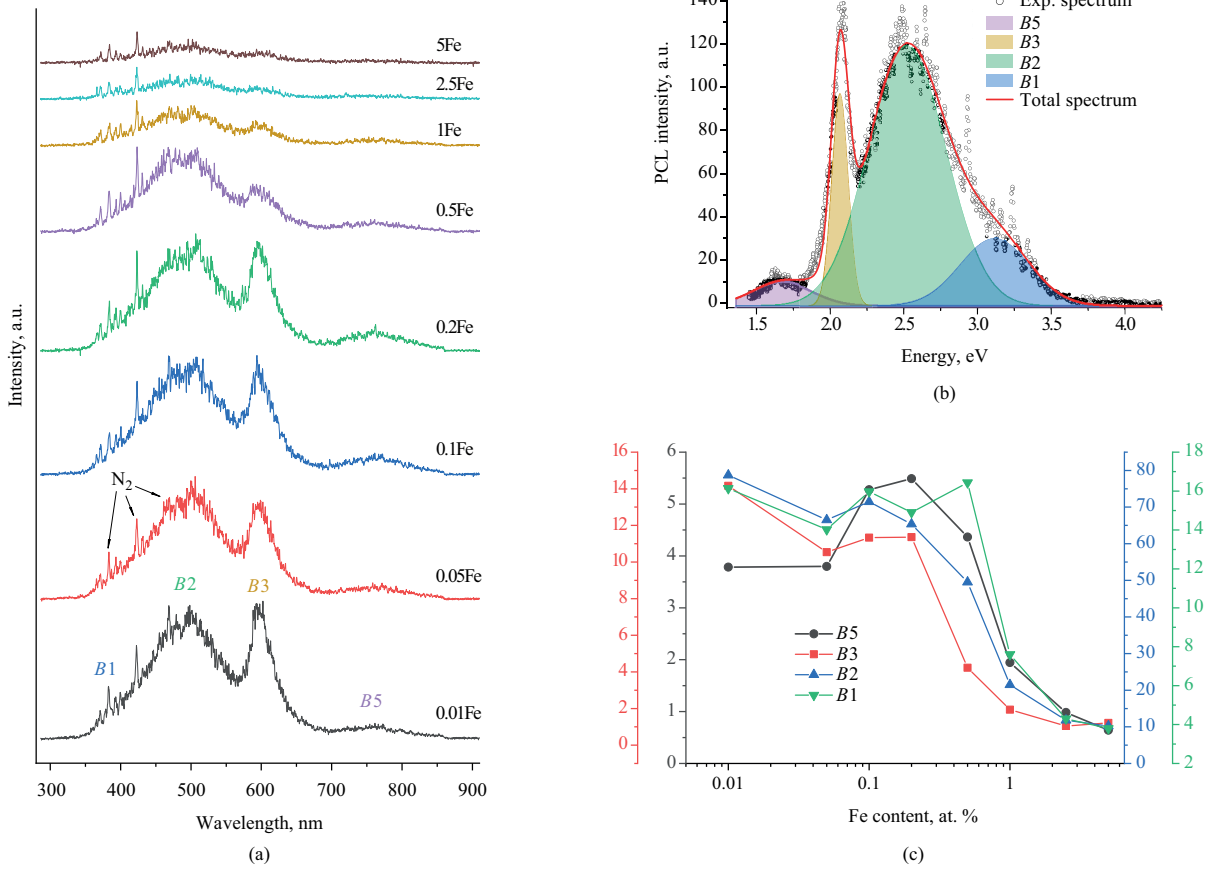

Fig. 9. (a) PCL spectra of AlON:Fe samples; (b) decomposition of PCL spectrum of AlON:0.01Fe by 4 Gaussian bands; (c) dependence of the intensity of *B*1, *B*2, *B*3, and *B*5 bands on the total iron content (reprinted from [70])

CONCLUSIONS

AlONs, in particular γ-AlON, whose composition is usually described by the formula $Al_{23}O_{27}N_5$ or Al_5O_6N, are promising materials not only for the manufacture of high-strength glasses, but also for use as matrices of phosphors. The main methods for producing aluminum oxynitrides include direct high-temperature interaction of aluminum oxide and nitride, direct nitriding and carbothermal reduction-nitriding. AlONs are doped with REM and TM ions both to improve sinterability and increase physical and mechanical characteristics, as well as to impart certain optical properties. To date, there is information on the use of oxides and other compounds of Mg, Y, La, Sc, La, Pr, Sm, Gd, Dy, Er, and Yb as sintering additives. Conversely, Eu^{2+}, Tb^{3+}, and Mn^{2+}, and in some cases Ce^{3+}, Er^{3+}, Sm^{3+}, Yb^{3+}, and Cr^{3+}, are more commonly used to impart luminescent properties. Double doping with Eu^{2+}/Ce^{3+}, Tb^{3+}/Eu^{2+}, and Tb^{3+}/Ce^{3+} ions can be used to adjust the luminescence color of the phosphor, as well as to reduce the content of terbium, one of the most expensive REMs, in phosphors due to the sensitization effect. Although doping with Ti, Co, and Fe ions does not impart luminescent properties, it facilitates the synthesis and processing of AlONs.

Acknowledgments

The work was carried out within the framework of State Assignment No. 075-00319-25-00.

Authors' contributions

N.S. Akhmadullina—generalization of data on synthesis and phase composition, preparation of the manuscript.

A.V. Ishchenko—summarizing data on luminescent properties.

Authors declare no conflicts of interest.

REFERENCES

1. Abyzov A.M. Aluminum oxide and alumina ceramics (Review). Part 1. Properties of Al_2O_3 and industrial production of dispersed Al_2O_3. *Novye ogneupory = New Refractories*. 2019;1:16–23 (in Russ.). https://doi.org/10.17073/1683-4518-2019-1-16-23
2. Yamaguchi G., Yanagida H. Study on the reductive spinel – a new spinel formula AlN–Al_2O_3 instead of the previous one Al_3O_4. *Bull. Chem. Soc. Jap.* 1959;32(11):1264–1265. https://doi.org/10.1246/bcsj.32.1264
3. McCauley J.W. A simple model for aluminum oxynitride spinels. *J. Am. Ceram. Soc.* 1978;61(7–8):372–373. https://doi.org/10.1111/j.1151-2916.1978.tb09336.x
4. McCauley J.W., Corbin N.D. Phase relations and reaction sintering of transparent cubic aluminum oxynitride spinel (ALON). *J. Am. Ceram. Soc.* 1979;62(9–10):476–479. https://doi.org/10.1111/j.1151-2916.1979.tb19109.x
5. McCauley J.W., Patel P., Chen M., Gilde G., Strassburger E., Paliwal B., Dandekar D.P. ALON: a brief history of its emergence and evolution. *J. Eur. Ceram. Soc.* 2009;29(2):223–236. https://doi.org/10.1016/j.jeurceramsoc.2008.03.046
6. McCauley J.W., Corbin N.D. High Temperature Reactions and Microstructures in the Al_2O_3-AlN System. In: Riley F.L. (Ed.). *Progress in Nitrogen Ceramics. NATO ASI Series*. Springer; 1983. V. 65. P. 111–118. https://doi.org/10.1007/978-94-009-6851-6_8
7. Batyrev I.G., Taylor D.E., Gazonas G.A., McCauley J.W. Density functional theory and evolution algorithm calculations of elastic properties of AlON. *J. Appl. Phys.* 2014;115(2):023505. https://doi.org/10.1063/1.4859435
8. Swab J.J., LaSalvia J.C., Gilde G.A., Patel P.J., Motyka M.J. Transparent armor ceramics: Alon and spinel. *Ceram. Eng. Sci. Proc.* 1999;20(4):79–84. https://doi.org/10.1002/9780470294574.ch10
9. Maguire E.A., Rawson J.K., Tustison R.W. Aluminum oxynitride's resistance to impact and erosion. In: *SPIE's 1994 Int. Symposium on Optics, Imaging, and Instrumentation. Proc. SPIE*. 1994;2286:26–32. https://doi.org/10.1117/12.187372
10. Kargin Yu.F., Akhmadullina N.S., Solntsev K.A. Ceramic Materials and Phosphors Based on Silicon Nitride and SiALON. *Inorg. Mater.* 2014;50(13):1325–1342. https://doi.org/10.1134/S0020168514130032
11. Shang M., Geng D., Yang D., Kang X., Zhang Y., Lin J. Luminescence and energy transfer properties of $Ca_2Ba_3(PO_4)_3Cl$ and $Ca_2Ba_3(PO_4)_3Cl$:A (A = $Eu^{2+}/Ce^{3+}/Dy^{3+}/Tb^{3+}$) under UV and low-voltage electron beam excitation. *Inorg. Chem.* 2013;52(6):3102–3112. https://doi.org/10.1021/ic3025759
12. Liu H., Luo Y., Mao Z., Liao L., Xia Z. A novel single-composition trichromatic white-emitting $Sr_{3.5}Y_{6.5}O_2(PO_4)_{1.5}(SiO_4)_{4.5}$: $Ce^{3+}/Tb^{3+}/Mn^{2+}$ phosphor: synthesis, luminescent properties and applications for white LEDs. *J. Mater. Chem. C.* 2014;2(9):1619–1627. https://doi.org/10.1039/C3TC32003K
13. Lin C.C., Liu R.S. Advances in phosphors for light-emitting diodes. *J. Phys. Chem. Lett.* 2011;2(11):1268–1277. https://doi.org/10.1021/jz2002452
14. Yamamoto H. White LED phosphors: the next step. *Proc. SPIE*. 2010;7598:08–14. https://doi.org/10.1117/12.843536
15. Bachmann V., Ronda C., Meijerink A. Temperature quenching of yellow Ce^{3+} luminescence in YAG:Ce. *Chem. Mater.* 2009;21(10):2077–2084. http://dx.doi.org/10.1021/cm8030768
16. Setlur A.A. Phosphors for LED-based solid-state lighting. *Electrochem. Soc. Interface*. 2009;18(4):32–36. http://dx.doi.org/10.1149/2.F04094IF
17. Xia Z.G., Wang X.M., Wang Y.X., Liao L.B., Jing X.P. Synthesis, structure, and thermally stable luminescence of Eu^{2+}-doped $Ba_2Ln(BO_3)_2Cl$ (Ln = Y, Gd and Lu) host compounds. *Inorg. Chem.* 2011;50(20):10134–10142. https://doi.org/10.1021/ic200988w
18. Zhu G., Wang Y., Ci Z., Liu B., Shi Y., Xin S. $Ca_5La_5(SiO_4)_3(PO_4)_3O_2$: Ce^{3+},Mn^{2+}: A color-tunable phosphor with efficient energy transfer for white light-emitting diodes. *J. Electrochem. Soc.* 2011;158:J236–J242. https://doi.org/10.1149/1.3595434

19. Fukuyama H., Nakao W., Susa M., Nagata K. New synthetic method of forming aluminum oxynitride by plasma arc melting. *J. Am. Ceram. Soc.* 1999;82(6):1381–1387. https://doi.org/10.1111/j.1151-2916.1999.tb01927.x
20. Rafaniello W., Cutler I.B. Preparation of sinterable cubic aluminum oxynitride by the carbothermal nitridation of aluminum-oxide. *J. Am. Ceram. Soc.* 1981;64(10):128–C128. https://doi.org/10.1111/j.1151-2916.1981.tb10232.x
21. Zientara D., Bućko M.M., Lis J. ALON-based materials prepared by SHS technique. *J. Eur. Ceram. Soc.* 2007;27(2–3): 775–779. https://doi.org/10.1016/j.jeurceramsoc.2006.04.008
22. Wang S.F., Zhang J., Luo D.W., Gua F., Tang D.Y., Dong Z.L., Kong L.B. Transparent ceramics: Processing, materials and applications. *Prog. Sol. State Chem.* 2013;41:20–54. https://doi.org/10.1016/j.progsolidstchem.2012.12.002
23. Patel P.J., Gilde G., McCauley J.W. The role of gas pressure in transient liquid phase sintering of aluminum oxynitride (Alon). *Cer. Eng. Sci. Proc.* 2003;24(3):425–431. https://doi.org/10.1002/9780470294802.ch61
24. Martin C., Cales B. Synthesis and Hot Pressing Of Transparent Aluminum Oxynitride. In: *SPIE 1989 Technical Symposium on Aerospace Sensing*. *Proc. SPIE;* 1989. V. 1112. P. 20–24. https://doi.org/10.1117/12.960759
25. Jin X., Gao L., Sun J., Liu Y., Gui L. Highly Transparent AlON Pressurelessly Sintered from Powder Synthesized by a Novel Carbothermal Nitridation Method. *J. Am. Ceram. Soc.* 2012;95(9): 2801–2807. https://doi.org/10.1111/j.1551-2916.2012.05253.x
26. Wang J., Zhang F., Chen F., Zhang J., Zhang H., Tian R., Wang Z., Liu J., Zhang Z., Chen S., Wang S. Effect of Y_2O_3 and La_2O_3 on the sinterability of γ-AlON transparent ceramics. *J. Eur. Ceram. Soc.* 2015;35(1):23–28. https://doi.org/10.1016/j.jeurceramsoc.2014.07.016
27. Tsukuma K. Transparent $MgAl_2O_4$ Spinel Ceramics Produced by HIP Post-Sintering. *J. Ceram. Soc. Jap.* 2006;114(1334): 802–806. https://doi.org/10.2109/jcersj.114.802
28. Chen F., Zhang F., Wang J., Zhang H., Tian R., Zhang J., Zhang Z., Sun F., Wang S. Microstructure and optical properties of transparent aluminum oxynitride ceramics by hot isostatic pressing. *Scripta Mater.* 2014;81:20–23. https://doi.org/10.1016/j.scriptamat.2014.02.009
29. Chen F., Zhang F., Wang J., Zhang H., Tian R., Zhang Z., Wang S. Hot isostatic pressing of transparent AlON ceramics with Y_2O_3/La_2O_3 additives. *J. Alloys Compd.* 2015;650: 753–757. https://doi.org/10.1016/j.jallcom.2015.08.028
30. Zhang J., Lei J., Shi Y., Xie J., Lei F., Zhang L. Effect of Y_2O_3, La_2O_3 and MgO Co-Doping on Densification, Microstructure and Properties of AlON Ceramics. *J. Ceram. Sci. Tech.* 2017;8(1):177–182. https://dx.doi.org/10.4416/JCST2016-00114
31. Dong Q., Yang F., Cui J., Tian Y., Liu S., Du F., Peng J., Ye X. Enhanced narrow green emission and thermal stability in γ-AlON:Mn^{2+},Mg^{2+} phosphor via charge compensation. *Ceram. Int.* 2019;45(9): 11868–11875. https://doi.org/10.1016/j.ceramint.2019.03.069
32. Thi M.H.N., Le P.X. Utilizing a strait-range green phosphor γ-AlON: Mn,Mg for the task of achieving a super-broad hue gamut display. *Indones. J. Electr. Eng. Comput. Sci.* 2022;27(2): 748–753. http://doi.org/10.11591/ijeecs.v27.i2.pp748-753
33. Kikkawa S., Hatta N., Takeda T. Preparation of Aluminum Oxynitride by Nitridation of a Precursor Derived from Aluminum–Glycine Gel and the Effects of the Presence of Europium. *J. Am. Ceram. Soc.* 2008;91(3):924–928. https://doi.org/10.1111/j.1551-2916.2007.02213.x
34. Yin L., Xu X., Hao L., Xie W., Wang Y., Yang L., Yang X. Synthesis and photoluminescence of Eu^{2+}–Mg^{2+} co-doped γ-AlON phosphors. *Mater. Lett.* 2009;63(17):1511–1513. https://doi.org/10.1016/j.matlet.2009.04.002
35. Zhang F., Chen S., Chen J.F., Zhang H.L., Li J., Liu X.J., Wang S.W. Characterization and luminescence properties of AlON:Eu^{2+} phosphor for white-emitting-diode illumination. *J. Appl. Phys.* 2012;111(8):083532. https://doi.org/10.1063/1.4705404
36. Zhang L., Luo H., Zhou L., Liu Q., Li J., Zhang W. Preparation of γ-aluminum oxynitride phosphor with Eu doping by direct nitridation in ammonia and postannealing. *J. Am. Ceram. Soc.* 2018;101(8):3299–3308. https://doi.org/10.1111/jace.15494
37. Akhmadullina N.S., Lysenkov A.S., Ashmarin A.A., Baranchikov A.E., Ishchenko A.V., Yagodin V.V., Shul'gin B.V., Kargin Yu.F. Synthesis and luminescence properties of Eu^{2+}- and Ce^{3+}-doped AlONs. *Ceram. Int.* 2016;42(1):286–293. https://doi.org/10.1016/j.ceramint.2015.08.107
38. Akhmadullina N.S., Ishchenko A.V., Yagodin V.V., *et al.* Synthesis and Luminescence Properties of Tb^{3+}-Doped Aluminum Oxynitride. *Inorg. Mater.* 2019;55(12):1223–1229. http://dx.doi.org/10.1134/S002016851912001X
[Original Russian Text: Akhmadullina N.S., Ishchenko A.V., Yagodin V.V., Lysenkov A.S., Sirotinkin V.P., Kargin Yu.F., Shulgin B.V. Synthesis and Luminescence Properties of Tb^{3+}-Doped Aluminum Oxynitride. *Neorganicheskie materialy.* 2019;55(12):1298–1304 (in Russ.). https://doi.org/10.1134/S0002337X19120017]
39. Akhmadullina N.S., Ishchenko A.V., Lysenkov A.V., Shishilov O.N., Kargin Yu.F. Synthesis and luminescence properties of Eu^{2+}/Ce^{3+}, Ce^{3+}/Tb^{3+} and Eu^{2+}/Tb^{3+} co-doped AlONs. *J. Alloys Compd.* 2021;887:161410. https://doi.org/10.1016/j.jallcom.2021.161410
40. Zorenko Y., Zorenko T., Voznyak T., Mandowski A., Xia Q., Batentschuk M., Friedrich J. Luminescence of F^+ and F centers in Al_2O_3-Y_2O_3 oxide compounds. *IOP Conf. Ser.: Mater. Sci. Eng.* 2010;15:012060. http://dx.doi.org/10.1088/1757-899X/15/1/012060
41. Trinkler L., Berzina B. Localised transitions in luminescence of AlN ceramics. *Radiat. Meas.* 2014;71:232–236. https://doi.org/10.1016/j.radmeas.2014.02.016
42. Weinstein I.A., Vokhmintsev A.S., Spiridonov D.M. Thermoluminescence kinetics of oxygen-related centners in AlN single crystals. *Diam. Relat. Mater.* 2012;25:59–62. https://doi.org/10.1016/j.diamond.2012.02.004
43. Zhang X., Li Z., Zeng Q. First-principles calculation on the electronic structure and optical properties of Eu^{2+} doped γ-AlON phosphor. *Ceram. Int.* 2018;44(2):1461–1466. https://doi.org/10.1016/j.ceramint.2017.10.044
44. French R.H. Electronic band structure of Al_2O_3, with comparison to AlON and AIN. *J. Am. Ceram. Soc.* 1990;73(3):477–489. https://doi.org/10.1111/j.1151-2916.1990.tb06541.x
45. Thomas M.E., Tropf W.J., Gilbert S.L. Vacuum-ultraviolet characterization of sapphire ALON, and spinel near the band gap. *Opt. Eng.* 1993;32(6):1340–1343. https://doi.org/10.1117/12.135837
46. Chen C.-F., Yang P., King G., Tegtmeier E.L. Processing of Transparent Polycrystalline AlON:Ce^{3+} Scintillators. *J. Am. Ceram. Soc.* 2016;99(2):424–430. https://doi.org/10.1111/jace.13986
47. Hu W.-W., Zhu Q.-Q., Hao L.-Y., Xu X., Agathopoulos S. Luminescence properties and energy transfer in Al_5O_6N:Ce^{3+},Tb^{3+} phosphors. *J. Luminesc.* 2014;149:155–158. https://doi.org/10.1016/j.jlumin.2014.01.010
48. Cavalli E., Boutinaud P., Mahiou R., Bettinelli M., Dorenbos P. Luminescence Dynamics in Tb^{3+}-Doped $CaWO_4$ and $CaMoO_4$ Crystals. *Inorg. Chem.* 2010;49(11):4916–4921. https://doi.org/10.1021/ic902445c

49. Baklanova Y.V., Maksimova L.G., Denisova T.A., Tyutyunnik A.P., Zubkov V.G. Synthesis and Luminescence Properties of Tb^{3+} and Dy^{3+} Doped $Li_7La_3Hf_2O_{12}$ with Tetragonal Garnet Structure. *Opt. Mater.* 2019;87:122–126. https://doi.org/10.1016/j.optmat.2018.04.041
50. Han B., Liang H., Huang Y., Tao Y., Su Q. Vacuum Ultraviolet–Visible Spectroscopic Properties of Tb^{3+} in $Li(Y,Gd)(PO_3)_4$: Tunable Emission, Quantum Cutting, and Energy Transfer. *J. Phys. Chem. C.* 2010;114(14):6770–6777. https://doi.org/10.1021/jp100755d
51. Zhang F., Wang S.W., Liu X.J., An L.Q., Yuan X.Y. Upconversion luminescence in Er-doped γ-AlON ceramic phosphors. *J. Appl. Phys.* 2009;105(9):093542. https://doi.org/10.1063/1.3125516
52. Zhang F., Chen S., Zhang H.L., Li J., Yang Y., Zhou G.H., Liu X.J., Wang S.W. Upconversion Luminescence of γ-AlON:Er^{3+} Phosphors with Mg^{2+} Co-Doping. *J. Am. Ceram. Soc.* 2012;95(1):27–29. https://doi.org/10.1111/j.1551-2916.2011.04916.x
53. Wang Y., Xie X., Qi J., Wang S., Wei N., Lu Z., Chen X., Lu T. Bifunctional behavior of Er^{3+} ions as the sintering additive and the fluorescent agent in Er^{3+} single doped γ-AlON transparent ceramics. *J. Luminsc*. 2016;175:203–206. https://doi.org/10.1016/j.jlumin.2016.02.039
54. Tsabit A.M., Kim M.-D., Yoon D.-H. Effects of various rare-earth additives on the sintering and transmittance of γ-AlON. *J. Eur. Ceram. Soc.* 2020;40(8):3235–3243. https://doi.org/10.1016/j.jeurceramsoc.2020.03.027
55. Tsabit A.M., Chung W.J., Lee H., Yoon D.-H. Fabrication and photoluminescence of γ-AlON:Sm and Yb. *J. Am. Ceram. Soc.* 2022;42(4):1348–1353. https://doi.org/10.1016/j.jeurceramsoc.2021.12.015
56. Liu R.S., Liu Y.H., Bagkar N.C., Hu S.F., Enhanced luminescence of $SrSi_2O_2N_2$:Eu^{2+} phosphors by codoping with Ce^{3+}, Mn^{2+}, and Dy^{3+} ions. *Appl. Phys. Lett*. 2007;91(6):061119. http://dx.doi.org/10.1063/1.2768916
57. Song X., Fu R., Agathopoulos S., He H., Zhao X., Li R., Luminescence and energy transfer mechanism in $SrSi_2O_2N_2$:Ce^{3+}, Eu^{2+} phosphors for white LEDs. *J. Electrochem. Soc.* 2010;157(2):J34–J38. https://doi.org/10.1149/1.3270491
58. Jian X., Wang H., Lee M.-H., Tian W., Chen G.-Z., Chen W.-Q., Ji W.-W., Xu X., Yin L.-J. Insight the Luminescence Properties of AlON: Eu, Mg Phosphor under VUV Excitation. *Mater*. 2017;10(7):723. https://doi.org/10.3390/ma10070723
59. Deng L., Lei J., Shi Y., Lin T., Ren Y., Xie J., Photoluminescence of Tb^{3+}/Ce^{3+} co-doped aluminum oxynitride powders. *Mater. Lett.* 2011;65(4):769–771. https://doi.org/10.1016/j.matlet.2010.11.027
60. Wu Q., Li Y., Wang X., Zhao Z., Wang C., Li H., Mao A., Wang Y. Novel optical characteristics of Eu^{2+} doped and Eu^{2+}, Ce^{3+} co-doped $LiSi_2N_3$ phosphors by gas-pressed sintering. *RSC Adv.* 2014;4(73):39030–39036. https://doi.org/10.1039/C4RA05502K
61. Chen L., Du F., Liang Y., Zhu Y., Xiao Y., Peng J. A study on photoluminescence and energy transfer of γ-AlON:Ce^{3+},Eu^{2+} phosphors for application in full-visible-spectrum LED lighting. *Displays.* 2022;71:102147. https://doi.org/10.1016/j.displa.2021.102147
62. Zhang J., Ma C., Wen Z., Du M., Long J., Ma R., Yuan X., Li J., Cao Y. Photoluminescence and energy transfer properties of Eu^{2+} and Tb^{3+} co-doped gamma aluminum oxynitride powders. *Opt. Mater.* 2016;58:290–295. https://doi.org/10.1016/j.optmat.2016.05.048
63. Xie R.-J., Hirosaki N., Liu X.-J., Takeda T., Li H.-L. Crystal Structure and Photoluminescence of Mn^{2+}, Mg^{2+} Codoped Gamma Aluminum Oxynitride (γ-AlON): A Promising Green Phosphor for White Light-Emitting Diode. *Appl. Phys. Lett.* 2008;92(20):201905. https://doi.org/10.1063/1.2920190
64. Kitaura M., Harima A., Xie R.-J., Takeda T., Hirosaki N., Ohnishi A., Sasaki M. Electron Spin Resonance Study on Local Structure of Manganese Ions Doped in Gamma-Aluminum Oxynitride Phosphors. *J. Light & Vis. Env.* 2012;36(1):6–9. https://doi.org/10.2150/jlve.36.6
65. Hao L., Miao X., Li K., Zhong J., Tu B., Yang Z., Wang H. Structural and Luminescent Properties of $Mg_{0.25-x}Al_{2.57}O_{3.79}N_{0.21}$:$xMn^{2+}$ Green-Emitting Transparent Ceramic Phosphor. *J. Wuhan Univ. Technol.-Mat. Sci. Edit*. 2024;39(3):533–540. https://doi.org/10.1007/s11595-024-2909-3
66. Zhou X., Chen S., Zhang C., Huang X., Lu K., Qi L., Lu T. Mn^{2+}/Mg^{2+} co-doped AlON ceramic with ultra-narrowband green emission combining high transparency toward a wide gamut backlight application. *Opt. Lett.* 2024;49(9):2245–2248. https://doi.org/10.1364/OL.520495
67. Liu L., Zhang J., Wang X., Hou W., Liu X., Xu M., Yang J., Liang B. Preparation and fluorescence properties of a Cr^{3+}:γ-AlON powder by high temperature solid state reaction. *Mater. Lett.* 2020;258:126811. https://doi.org/10.1016/j.matlet.2019.126811
68. Ishchenko A.V., Akhmadullina N.S., Leonidov I.I., Sirotinkin V.P., Skvortsova L.G., Shishilov O.N., Zhidkov I.S., Kukharenko A.I., Kargin Yu.F. Synthesis and spectroscopic properties of aluminum oxynitride doped with 3d-metal ions: The case of γ-AlON:Ti. *J. Alloys Compd.* 2023;934:167792. https://doi.org/10.1016/j.jallcom.2022.167792
69. Ishchenko A.V., Akhmadullina N.S., Leonidov I.I., Sirotinkin V.P., Skvortsova L.G., Mandrygina D.A., Shishilov O.N., Zhidkov I.S., Kukharenko A.I., Weinstein I.A., Kargin Yu.F. Synthesis, phase composition, electronic and spectroscopic properties of cobalt-doped aluminum oxynitride. *Physica B: Condens. Matter*. 2024;695:416593. https://doi.org/10.1016/j.physb.2024.416593
70. Ishchenko A.V., Akhmadullina N.S., Pastukhov D.A., *et al.* Phase composition and optical properties of Fe-doped aluminum oxynitride. *Inorg. Mater.* 2024;60(3):859–866. https://doi.org/10.1134/S002016852470119X
[Original Russian Text: Ishchenko A.V., Akhmadullina N.S., Pastukhov D.A., Leonidov I.I., Sirotinkin V.P., Lysenkov A.S., Shishilov O.N., Kargin Yu.F. Phase composition and optical properties of Fe-doped aluminum oxynitride. *Neorganicheskie materialy.* 2024;60(3):322–330 (in Russ.).]
71. Kubelka P., Munk F. Ein beitrag zur optik der farbanstriche. *Z. Tech. Phys.* 1931;12:593–601.
72. Du X., Yao S., Jin X., Chen H., Li W., Liang B. Radiation damage and luminescence properties of gamma aluminum oxynitride transparent ceramic. *J. Phys. D.: Appl. Phys.* 2015;48(34):345104. https://doi.org/10.1088/0022-3727/48/34/345104
73. Tauc J. Optical properties and electronic structure of amorphous Ge and Si. *Mater. Res. Bull.* 1968;3(1):37–46. https://doi.org/10.1016/0025-5408(68)90023-8
74. Xu J., Cherepy N.J., Ueda J., Tanabe S. Red persistent luminescence in rare earth- free AlN:Mn^{2+} phosphor. *Mater. Lett.* 2017;206:175–177. https://doi.org/10.1016/j.matlet.2017.07.015
75. Zorenko Y., Zorenko T., Voznyak T., Nizhankovskiy S., Krivonosov E., Danko A., Puzikov V., Comparative study of the luminescence of Al_2O_3:Ti and Al_2O_3 crystals under VUV synchrotron radiation excitation. *Opt. Mater.* 2013;35(12):2053–2055. https://doi.org/10.1016/j.optmat.2012.10.044

76. Gaffney E.S. Spectra of tetrahedral Fe^{2+} in $MgAl_2O_4$. *Phys. Rev. B*. 1973;8:3484–3486. https://doi.org/10.1103/PhysRevB.8.3484
77. Basyrova L., Bukina V., Balabanov S., Belyaev A., Drobotenko V., Dymshits O., Alekseeva I., Tsenter M., Zapalova S., Khubetsov A., Zhilin A., Volokitina A., Vitkin V., Mateos X., Serres J.M., Camy P., Loiko P. Synthesis, structure and spectroscopy of Fe^{2+}:$MgAl_2O_4$ transparent ceramics and glass-ceramics. *J. Lumin.* 2021;236:118090. https://doi.org/10.1016/j.jlumin.2021.118090
78. Thi Le T.-L., Nguyen L.T., Nguyen H.-H., Van Nghia N., Vuong N.M., Hieu H.N., Van Thang N., Le V.T., Nguyen V.H., Lin P.-C., Yadav A., Madarevic I., Janssens E., Van Bui H., Ngoc L.L.T. Titanium nitride nanodonuts synthesized from natural ilmenite ore as a novel and efficient thermoplasmonic material. *Nanomaterials*. 2021;11(1):76. https://doi.org/10.3390/nano11010076
79. Taborda J.A.P., Landázuri H.R., Londoño L.P.V. Correlation Between Optical, Morphological, and Compositional Properties of Aluminum Nitride Thin Films by Pulsed Laser Deposition. *IEEE Sens. J*. 2016;16(2):359–364. https://doi.org/10.1109/JSEN.2015.2466467
80. Prieto P., Kirby R.E. X-ray photoelectron spectroscopy study of the difference between reactively evaporated and direct sputter-deposited TiN films and their oxidation properties. *J. Vac. Sci. Technol. A*. 1995;13(6):2819–2826. https://doi.org/10.1116/1.579711

About the Authors

Nailya S. Akhmadullina, Cand. Sci. (Chem.), Senior Researcher, Laboratory of Physical and Chemical Analysis of the Ceramic Materials, A.A. Baikov Institute of Metallurgy and Material Science of the Russian Academy of Sciences (49, Leninskii pr., Moscow, 119991, Russia). E-mail: nakhmadullina@mail.ru. Scopus Author ID 26432528700, ResearcherID M-7540-2018, RSCI SPIN-code 4892-2471, https://orcid.org/0000-0002-5662-1223

Alexey V. Ishchenko, Cand. Sci. (Phys.-Math.), Associate Professor, Senior Researcher, Department of Experimental Physics, Ural Federal University (19, Mira pr., Yekaterinburg, 620062, Russia). E-mail: a-v-i@mail.ru. Scopus Author ID 57195266830, RSCI SPIN-code 3652-5774, https://orcid.org/0000-0002-9883-6652

Об авторах

Ахмадуллина Наиля Сайфулловна, к.х.н., старший научный сотрудник, лаборатория физико-химического анализа керамических материалов, ФГБУН «Институт металлургии и материаловедения им. А.А. Байкова Российской академии наук» (119991, Россия, Москва, Ленинский пр., д. 49). E-mail: nakhmadullina@mail.ru. Scopus Author ID 26432528700, ResearcherID M-7540-2018, SPIN-код РИНЦ 4892-2471, https://orcid.org/0000-0002-5662-1223

Ищенко Алексей Владимирович, к.ф.-м.н., доцент, старший научный сотрудник, кафедра экспериментальной физики, ФГАОУ ВО «Уральский федеральный университет имени первого Президента России Б.Н. Ельцина» (620062, Россия, Екатеринбург, пр. Мира, д. 19). E-mail: a-v-i@mail.ru. Scopus Author ID 57195266830, SPIN-код РИНЦ 3652-5774, https://orcid.org/0000-0002-9883-6652

Translated from Russian into English by H. Moshkov
Edited for English language and spelling by Thomas A. Beavitt